TABLE II. Measurements of Cardiac Functions

Tests	Measurements	Number of subjects	Results mean ± SD (range)	Number of abnormal subjects
ECG	At rest	61	Normal	0
	After exercise	61	ST elevation	1
Holter ECG	Arrhythmia	59	SVPC	2
	CVNN (%)	59	19.8 ± 3.2 (2.7–27.1)	0
Echocardiography	LVDd (mm)	61	43.9 ± 4.0 (36.1–52.0)	0
	LVDs (mm)	61	26.9 ± 3.4 (19.0–34.6)	0
	EF (%)	61	70.4 ± 6.2 (53.0–81.3)	1
	FS (%)	61	38.7 ± 4.6 (29.4–50.0)	0
	E/A ratio	48	2.08 ± 0.47 (1.43–4.0)	0
6MWT	Total (m)	41	563.4 ± 142.5	5
	Males (m)	18	650.4 ± 110.9 (362.0–904.5)	1
	Females (m)	23	495.4 ± 126.7 (252.0–699.6)	4
Laboratory exercise testing	BNP at rest (pg/ml)	60	13.3 ± 14.6 (2.0–70.8)	6
	BNP after exercise (pg/ml)	60	15.1 ± 15.4 (2.0–85.2)	6

6MWT, 6-min walk test; CVNN, co-variance of NN intervals; LVDd, left ventricular end-diastolic dimension; LVDs, left ventricular end-systolic dimension; EF, ejection fraction; FS, fractional shortening; SVPC, supra-ventricular premature contraction.

TABLE III. Plasma BNP Levels in Patients and Controls

	BNP (pg/ml)		
	At rest	After exercise	Difference
Patients (n = 60)	13.3 ± 14.7	15.1 ± 15.5	1.8 ± 8.7
Control (n = 10)	10.7 ± 9.3	11.1 ± 10.5	0.4 ± 1.8
P	0.60	0.53	0.63

Values are expressed as mean ± SD.

subjects. Echocardiographic studies showed no cardiac dysfunction, and abnormal measurement was recorded in only one subject with a subnormal EF value of 53%. The 6MWT was performed on 41 subjects, and a significantly short distance as compared to the standard values adjusted to sex and age was recorded in 5 (one male and 4 females). The elevated plasma BNP levels defined as greater than the mean + 2 SD of the 10 healthy controls were >28.3 pg/ml (before exercise) and >31.1 pg/ml (after exercise), respectively. Based on this criterion, abnormal BNP levels were detected in six subjects whose values were elevated both at rest and after exercise. The mean BNP values before and after exercise in patients and control subjects are shown in Table III, revealing no significant difference between the patients and controls.

Overall, some abnormal cardiac measurements were detected in 14 subjects, and the type of abnormality and cumulative AC dose for each subject are shown in Table IV.

Table V shows the correlation between cumulative THP dose and various cardiac measurements. The cumulative dose showed a significant correlation with plasma BNP levels after exercise (Fig. 1), but not with any other cardiac measurements. Further analysis of the plasma BNP levels after exercise revealed that 21 subjects who received a high cumulative dose $\geqq 300$ mg/m^2 of THP had significantly higher BNP levels as compared with 39 other subjects who received a low cumulative dose <300 mg/m^2 (Table VI). This table also shows increments in BNP levels (ΔBNP) after exercise compared to base-line values (at rest) between the two groups. A significant rise in ΔBNP after exercise

TABLE IV. Cumulative Dose of Anthracyclins and Abnormal Cardiac Measurements

Case	Cumulative dose of anthracyclins (DOX/THP) (mg/m^2)	Exercise ECG	Holter ECG	6MWT	Plasma BNP	
					At rest	After exercise
1	25/180	−	+	−	−	−
2	0/180	−	−	+	−	−
3	25/160	−	−	−	+	+
4	75/600	−	−	−	+	+
5	75/730	+	−	−	−	−
6	75/150	−	+	−	−	−
7	75/120	−	−	+	−	−
8	75/740	−	−	−	+	+
9	75/590	−	−	−	+	+
10	15/160	−	−	−	+	+
11	0/135	−	−	−	+	+
12	25/180	−	−	+	−	−
13	25/180	−	−	+	−	−
14	75/740	−	−	+	−	−

+ and − denote positive and negative results for cardiac measurements, respectively. DOX, doxorubicin; THP, pirarubicin.

TABLE V. Correlation of Cardiac Measurements and Total Dose of THP

Measurements	Correlation coefficient	*P*
FS	0.01	0.09
EF	0.90	0.49
E/A ratio	0.08	0.57
CVNN	0.26	0.08
6MWT	0.02	0.88
BNP at rest	0.11	0.42
BNP after exercise	0.27	0.03

THP, pirarubicin; FS, fractional shortening; EF, ejection fraction. CVNN, co-variance of NN intervals; 6MWT, 6-min walk test.

was observed for subjects with $\geqq 300$ mg/m^2 of THP, but not for subjects with <300 mg/m^2 of THP. Although correlations between the measurements of left ventricular function (FS and EF) and cumulative THP dose or BNP levels were studied, no significant results were obtained (Supplemental Appendix).

DISCUSSION

THP is a derivative of DOX developed in Japan, and its cardiotoxicity may be lower than that of DOX [12–15]. Tsurumi et al. and Niitsu et al. reported that acute cardiotoxicity with THP was less frequent than that with DOX among adult lymphoma patients [17–20]. However, no studies for late cardiotoxicity of THP have been reported. In this study, cardiac function and biomarkers were measured in long-term survivors with ALL who received THP treatment and in whom no apparent cardiac dysfunction was detected. Thus, this is the first report of late cardiotoxicity of THP in cancer survivors.

The incidence of AC-induced cardiac dysfunction in childhood cancer survivors varied considerably across studies. The incidences of 14–24% for cardiac dysfunction assessed by echocardiography had been reported in five studies, in which median doses of cumulative AC ranged from 165 to 450 mg/m^2 [6,7,28,29,31]. Three other studies also reported that cumulative AC dose was significantly associated with reduced FS function, and high cumulative dose >300 mg/m^2 increased the risk of cardiac dysfunction [11,26,27]. When our results are compared with these findings, it appears that incidence of cardiac dysfunction after THP treatment

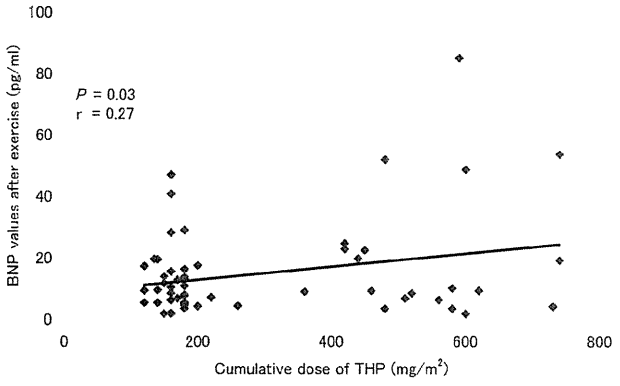

Fig. 1. Correlation between plasma BNP values after exercise and cumulative pirarubicin (THP) dose.

TABLE VI. Plasma BNP Levels According to Total Dose of THP

Total dose of THP	<300 mg/m^2 (n = 39)	$\geqq 300$ mg/m^2 (n = 21)	*P* value vs. <300 mg/m^2
BNP at rest (pg/ml)	12.5 ± 13.8	14.8 ± 15.8	0.56
BNP after exercise (pg/ml)	12.2 ± 9.9	20.6 ± 21.2	0.04
ΔBNP (pg/ml)	−0.3 ± 7.8	5.4 ± 8.1	0.01

Values are expressed as mean ± SD. THP, pirarubicin.

is relatively low. However, it should be noted that EF and FS may not be sensitive parameters for monitoring cardiac injury, because they often remain normal until critical point in the face of cardiac compensation [30]. Tissue Doppler echocardiography (TDE) has became widely available. Since TDE gives a more precise estimation for diastolic dysfunction than the E/A ratio used in this study, it may be helpful in future studies [40].

Non-invasive techniques for identifying patients who are at high-risk of developing AC-induced cardiomyopathy are critically important. For this purpose, natriuretic peptides including BNP and N-terminal fragment of BNP pro-hormone (NT-pro-BNP), are currently used for detection of cardiac injury in both adults and children [41]. Until now, 4 studies have reported BNP levels in childhood cancer survivors who received AC therapy [28–31]. In 3 of these, elevated BNP levels were detected [28,30,31], although the values did not significantly correlate with cumulative AC doses. Our study showed no significantly different BNP levels in patients from controls, but BNP levels after exercise were significantly correlated to cumulative THP dose. A similar finding was reported by Pinarli et al. [30], in which they found high BNP levels after exercise by treadmill, but no correlation with cumulative AC dose. Since augmented response in plasma BNP levels to exercise has been reported in adult patients with left ventricular dysfunction or exercise-induced ischemia [42,43], the increased BNP levels and ΔBNP after exercise in our study may be associated with subclinical myocardial injury. The stability of BNP in blood samples should be considered when interpreting BNP values after exercise. McNairy at al. found that post-exercise BNP returned to baseline levels within 60 min for normal subjects [44]. On the other hand, NT-pro-BNP is characterized by its stability against protease and longer half-life in comparison with BNP. Thus, the measurement of NT-pro-BNP may provide additional evidence in the early detection of anthracycline-induced cardiotoxicity in childhood and adolescence.

Currently, the 6MWT is considered to represent the most suitable method to assess the exercise tolerance. This self-paced test is easy to perform, well tolerated, and highly acceptable to children [39,45]. In our study, all subjects finished the test without difficulty or premature stopping. Consequently, the 6MWT may be used both in assessment and follow up of functional capacity in childhood cancer survivors.

In conclusion, the present study suggested that THP-induced late cardiac dysfunction is rare. However, further investigation is warranted to clarify the pathopsysiological significance of elevated BNP levels after the exercise test in asymptomatic patients.

ACKNOWLEDGMENT

We thank the patients who enrolled in this study and their families, and Paul Lewis for preparation of the manuscript.

REFERENCES

1. Hitchcock-Bryan S, Gelber R, Cassady JR, et al. The impact of induction anthracycline on long-term failure-free survival in childhood acute lymphoblastic leukemia. Med Pediatr Oncol 1986;14: 211–215.
2. Smith MA, Ungerleider RS, Horowitz ME, et al. Influence of doxorubicin dose intensity on response and outcome for patients with osteogenic sarcoma and Ewing's sarcoma. J Natl Cancer Inst 1991;83:1460–1470.
3. Giantris A, Abdurrahman L, Hinkle A, et al. Anthracycline-induced cardiotoxicity in children and young adults. Crit Rev Oncol Hematol 1998;27:53–68.
4. Scully RE, Lipshultz SE. Anthracycline cardiotoxicity in long-term survivors of childhood cancer. Cardiovasc Toxicol 2007;7: 122–128.
5. Beneficial and harmful effects of anthracyclines in the treatment of childhood acute lymphoblastic leukaemia: A systematic review and meta-analysis. Childhood Acute Lymphoblastic Leukaemia Collaborative Group (CALLCG). Br J Haematol 2009;145:376–388.
6. Lipshultz SE, Colan SD, Gelber RD, et al. Late cardiac effects of doxorubicin therapy for acute lymphoblastic leukemia in childhood. N Engl J Med 1991;324:808–815.
7. Steinherz LJ, Steinherz PG, Tan CT, et al. Cardiac toxicity 4–20 years after completing anthracycline therapy. JAMA 1991;266: 1672–1677.
8. Krischer JP, Epstein S, Cuthbertson DD, et al. Clinical cardiotoxicity following anthracycline treatment for childhood cancer: The Pediatric Oncology Group experience. J Clin Oncol 1997; 15:1544–1552.
9. Kremer LC, van Dalen EC, Offringa M, et al. Anthracycline-induced clinical heart failure in a cohort of 607 children: Long-term follow-up study. J Clin Oncol 2001;19:191–196.
10. Sorensen K, Levitt GA, Bull C, et al. Late anthracycline cardiotoxicity after childhood cancer: A prospective longitudinal study. Cancer 2003;97:1991–1998.
11. Lipshultz SE, Lipsitz SR, Sallan SE, et al. Chronic progressive cardiac dysfunction years after doxorubicin therapy for childhood acute lymphoblastic leukemia. J Clin Oncol 2005; 23:2629–2636.
12. Umezawa H, Takahashi Y, Kinoshita M, et al. Tetrahydropyranyl derivatives of daunomycin and adriamycin. J Antibiot 1979;32: 1082–1084.
13. Takagi T, Oguro M. (2-R)-4-o-Tetrahydropyranyladriamycin, a new anthracyclin derivative; its effectiveness in lymphoid malignancies. Cancer Chemother Pharmacol 1987;20:151–154.
14. Takagi T, Sakai C, Oguro M. Combination chemotherapy with pirarubicin (THP), cyclophosphamide, vincristine, and prednisolone (VEP-THP therapy) in the treatment of non-Hodgkins lymphoma. Oncology 1990;47:25–28.
15. Miller AA, Salewski E. Prospects for pirarubicin. Med Pediatr Oncol 1994;22:261–268.
16. Aoki S, Tsukada N, Nomoto N, et al. Effect of pirarubicin for elderly patients with malignant lymphoma. J Exp Clin Cancer Res 1998;17:465–470.
17. Niitsu N, Umeda M. Biweekly THP-COPBLM (pirarubicin, cyclophosphamide, vincristine, prednisone, bleomycin and procarbazine) regimen combined with granulocyte colony-stimulating factor (G-CSF) for intermediate- and high-grade non-Hodgkins's lymphoma. Leukemia 1998;12:1457–1460.
18. Niitsu N, Umeda M. Response and adverse drug reactions to combination chemotherapy in elderly patients with aggressive non-Hodgkin's lymphoma: Comparison of CHOP, COP-BLAM, COP-BLAM III, and THP-COPBLM. Eur J Haematol 1999;63: 337–344.
19. Tsurumi H, Yamada T, Sawada M, et al. Biweekly CHOP or THP-COP regimens in the treatment of newly diagnosed aggressive non-Hodgkin's lymphoma. A comparison of doxorubicin and pirarubicin: A randomized phase II study. J Cancer Res Clin Oncol 2004;130:107–113.
20. Zhai L, Guo C, Cao Y, et al. Long-term results of pirarubicin versus doxorubicin in combination chemotherapy for aggressive non-Hodgkin's lymphoma: Single center, 15-year experience. Int J Hematol 2010;91:78–86.
21. Kawa K, Ohnuma N, Kaneko M, et al. Long-term survivors of advanced neuroblastoma with MYCN amplification: A report of 19 patients surviving disease-free for more than 66 months. J Clin Oncol 1999;17:3216–3220.
22. Kaneko M, Tsuchida Y, Mugishima H, et al. Intensified chemotherapy increases the survival rates in patients with stage 4 neuroblastoma with MYCN amplification. J Pediatr Hematol Oncol 2002;24:613–621.
23. Tsurusawa M, Taga T, Horikoshi Y, et al. Favourable outcomes in children with diffuse large B-cell lymphoma treated by a short-term ALL-like regimen: A report on the NHL960 study from the Japanese Childhood Cancer and Leukemia Study Group. Leuk Lymphoma 2008;49:734–739.
24. Tsurusawa M, Shimomura Y, Asami K, et al. Long-term results of the Japanese Childhood Cancer and Leukemia Study Group studies 811, 841, 874 and 911 on childhood acute lymphoblastic leukemia. Leukemia 2010;24:335–344.
25. Yamaji K, Okamoto T, Yokota S, et al. Minimal Residual Disease-based Augmented Therapy in Childhood Acute Lymphoblastic Leukemia: A Report from The Japanese Childhood Cancer and Leukemia Study Group Study. Pediatr Blood Cancer 2010;55: 1287–1295.
26. Lipshultz SE, Lipsitz SR, Mone SM, et al. Female sex and drug dose as risk factors for late cardiotoxic effects of doxorubicin therapy for childhood cancer. N Engl J Med 1995;332:1738–1743.
27. Nysom K, Holm K, Lipsitz SR, et al. Relationship between cumulative anthracycline dose and late cardiotoxicity in childhood acute lymphoblastic leukemia. J Clin Oncol 1998; 16: 545–550.
28. Hayakawa H, Komada Y, Hirayama M, et al. Late cardiac evaluation of children with solid tumors after anthracycline chemotherapy. Med Pediatr Oncol 2001;37:4–9.
29. Poutanen T, Tikanoja T, Riikonen P, et al. Long-term prospective follow-up study of cardiac function after cardiotoxic therapy for malignancy in children. J Clin Oncol 2003;21:2349–2356.
30. Pinarli FG, Oguz A, Tunaoglu FS, et al. Late cardiac evaluation of children with solid tumors after anthracycline chemotherapy. Pediatr Blood Cancer 2005;44:370–377.
31. Aggarwal S, Pettersen MD, Bhambhani K, et al. B-Type natriuretic peptide as a marker for cardiac dysfunction in anthracycline-treated children. Pediatr Blood Cancer 2007;49:812–816.
32. The criteria committee of the New York Heart Association. Nomenclature and criteria for diagnosis of diseases of the heart and great vessels, 9th edition. Boston, MA: Little, Brown & Co; 1994.
33. Fletcher GF, Balady GJ, Amsterdam EA, et al. Exercise standards for testing and training: A statement for healthcare professionals from the American Heart Association. Circulation 2001;104: 1694–1740.
34. Shimosaka K, Takahashi A, Saitou H, et al. Evaluation of automated chemiluminescent immunoassay analyzer exclusive kit "MI02 Shionogi BNP". Igaku to Yakugaku 2005;53:353–360 (in Japanese).

35. Sahn DJ, DeMaria A, Kisslo J, et al. Recommendations regarding quantification in M-mode echocardiography: Result of a survey of echocardiographic measurements. Circulation 1978; 58:1072–1083.
36. Kimball TR, Michelfelder EC. Echocardiography, in Moss & Adams's "Heart Disease in Infants, Children, and Adolescents", 8th edition. Philadelphia: Lippincott Williams & Wilkins; 2008, pp. 95–162.
37. Bu'Lock FA, Mott MG, Oakhill A, et al. Left ventricular diastolic filling patterns associated with progressive anthracycline-induced myocardial damage: A prospective study. Pediatr Cardiol 1999;20:252–263.
38. Dorup I, Levitt G, Sullivan I, et al. Prospective longitudinal assessment of late anthracycline cardiotoxicity after childhood cancer: The role of diastolic function. Heart 2004;90:1214–1216.
39. Geiger R, Strasak A, Treml B, et al. Six-minute walk test in children and adolescents. J Pediatr 2007;150:395–399.
40. Civilibal M, Caliskan S, Oflaz H, et al. Left ventricular function by 'conventional' and 'tissue Doppler' echocardiography in paediatric dialysis patients. Nephrology (Carlton) 2009;14:636–642.
41. Mavinkurve-Groothuis AM, Kapusta L, Nir A, et al. The role of biomarkers in the early detection of anthracycline-induced cardiotoxicity in children: A review of the literature. Pediatr Hematol Oncol 2008;25:655–664.
42. Kato M, Kinugawa T, Ogino K, et al. Augmented response in plasma brain natriuretic peptide to dynamic exercise in patients with left ventricular dysfunction and congestive heart failure. J Intern Med 2000;248:309–315.
43. Foote RS, Pearlman JD, Siegel AH, et al. Detection of exercise-induced ischemia by changes in B-type natriuretic peptides. J Am Coll Cardiol 2004;44:1980–1987.
44. McNairy M, Gardetto N, Clopton P, et al. Stability of B-type natriuretic peptide levels during exercise in patients with congestive heart failure: Implications for outpatient monitoring with B-type natriuretic peptide. Am Heart J 2002;143:406–411.
45. Moalla W, Gauthier R, Maingourd Y, et al. Six-minute walking test to assess exercise tolerance and cardiorespiratory responses during training program in children with congenital heart disease. Int J Sports Med 2005;26:756–762.

Lung Cancer 75 (2012) 66–72

Contents lists available at ScienceDirect

Lung Cancer

journal homepage: www.elsevier.com/locate/lungcan

ALK fusion gene positive lung cancer and 3 cases treated with an inhibitor for ALK kinase activity

Hideki Kimura[a,*], Takahiro Nakajima[a,d], Kengo Takeuchi[b], Manabu Soda[c], Hiroyuki Mano[c], Toshihiko Iizasa[a], Yukiko Matsui[a], Mitsuru Yoshino[a], Masato Shingyoji[a], Meiji Itakura[a], Makiko Itami[e], Dai Ikebe[e], Sana Yokoi[f], Hajime Kageyama[f], Miki Ohira[g], Akira Nakagawara[h]

[a] Division of Thoracic Diseases, Chiba Cancer Center, Chiba, Japan
[b] Pathology Project for Molecular Targets, Cancer Institute, Japanese Foundation for Cancer Research (JFCR), Koto, Tokyo, Japan
[c] Division of Functional Genomics, Jichi Medical University, Tochigi, Japan
[d] Division of Thoracic Surgery, Toronto General Hospital, University Health Network, Toronto, Canada
[e] Division of Pathology, Chiba Cancer Center, Japan
[f] Cancer Genome Center, Chiba Cancer Center Research Institute, Japan
[g] Laboratory of Cancer Genomics, Chiba Cancer Center Research Institute, Japan
[h] Chiba Cancer Center, Japan

ARTICLE INFO

Article history:
Received 16 October 2010
Received in revised form 24 May 2011
Accepted 30 May 2011

Key words:
ALK
EML4
KIF5B
Fusion gene
Lung cancer
EBUS
TBNA
Crizotinib
ALK inhibitor

ABSTRACT

Background: Anaplastic lymphoma kinase (ALK) fusion gene-positive lung cancer accounts for 4–5% of non-small cell lung carcinoma. A clinical trial of the specific inhibitor of ALK fusion-type tyrosine kinase is currently under way.

Methods: ALK fusion gene products were analyzed immunohistochemically with the materials obtained by surgery or by endobronchial ultrasound-guided transbronchial needle aspiration (EBUS-TBNA). The echinoderm microtubule-associated protein-like 4(EML4)-ALK or kinesin family member 5B (KIF5B)-ALK translocation was confirmed by the reverse transcription polymerase chain reaction (RT-PCR) and fluorescence in situ hybridization (FISH). After eligibility criteria were met and informed consent was obtained, 3 patients were enrolled for the Pfizer Study of Crizotinib (PF02341066), Clinical Trial A8081001, conducted at Seoul National University.

Results: Out of 404 cases, there were 14 of EML4-ALK non-small cell carcinoma (NSCLC) and one KIF5B-ALK NSCLC case (8 men, 7 women; mean age, 61.9 years, range 48–82). Except for 2 light smokers, all patients were non-smokers. All cases were of adenocarcinoma with papillary or acinar subtypes. Three were of stage IA, 5 of stage IIIA, 1 of stage IIIB and 6 of stage IV. Ten patients underwent thoracotomy, 3 received chemotherapy and 2 only best supportive care (BSC). One BSC and 2 chemotherapy cases were enrolled for the clinical trial. Patients with advanced stages who received chemotherapy or best supportive care were younger (54.0 ± 6.3) than those who were surgically treated (65.8 ± 10.1) ($p < 0.05$).

The powerful effect of ALK inhibitor on EML4-ALK NSCLC was observed. Soon after its administration, almost all the multiple bone and lymph node metastases quickly disappeared. Nausea, diarrhea and the persistence of a light image were the main side effects, but they diminished within a few months.

Conclusion: ALK-fusion gene was found in 3.7% (15/404) NSCLC cases and advanced disease with this fusion gene was correlated with younger generation. The ALK inhibitor presented in this study is effective in EML4-ALK NSCLC cases. A further study will be necessary to evaluate the clinical effectiveness of this drug.

1. Introduction

As the mechanisms of carcinogenesis become clearer, the target of cancer treatment is shifting from non-specific cytotoxic agents to specific agents that block key molecular events in the carcinogenesis of malignancy such as EGFR-TKI and anti-HER2 antibody (trastuzumab) [1–3]. Recently, Mano et al. [4–6] reported that a small inversion within chromosome 2p results in the formation of a fusion gene comprising portions of the

* Corresponding author at: Division of Thoracic Diseases, Chiba Cancer Center, 666-2, Nitona-cho, Chuo-ku, 260-8717 Chiba, Japan. Tel.: +81 43 264 5431; fax: +81 43 262 8680.
E-mail address: hkimura@chiba-cc.jp (H. Kimura).

0169-5002/$ – see front matter © 2011 Elsevier Ireland Ltd. All rights reserved.
doi:10.1016/j.lungcan.2011.05.027

echinoderm microtubule-associated protein-like 4 (EML4) gene and the anaplastic lymphoma kinase (ALK) gene in non-small-cell lung cancer. Transgenic mice that express EML4-ALK specifically in lung epithelial cells develop multiple foci of adenocarcinoma in the lung soon after birth, and the oral administration of a specific inhibitor of ALK tyrosine kinase activity eradicated completely the foci of adenocarcinoma. Clinical trials of specific inhibitors of EML4-ALK tumors are currently underway [7–11]. Kwak et al. [11] reported the effect of crizotinib in Clinical Trial A8081001 on the 82 patients with advanced ALK-positive disease. Over a mean treatment duration of 6.4 months, the overall response rate was 57% and the estimated probability of 6-month progression-free survival was 72%. We report 15 cases of ALK fusion gene-positive NSCLC cases and 3 cases in our experience with ALK inhibitor in the Pfizer Study of crizotinib (PF02341066), Clinical Trial A8081001, which was conducted at Seoul National University.

2. Materials and methods

Out of 404 patients who had undergone surgical resection (295 cases) or bronchoscopy (109 cases) in Chiba Cancer Center, Japan, from 2007 to 2009, 15 ALK fusion gene-positive NSCLC patients were initially screened by immunohistochemical procedures. Diagnoses were confirmed by RT-PCR and/or FISH for their molecular translocation.

2.1. ALK fusion protein detection by immunohistochemical methods

The intercalated antibody-enhanced polymer method of Takeuchi et al. [12,13] was used to detect ALK proteins. Formalin-fixed paraffin-embedded tissue was sliced at a thickness of 4 μm and the sections were placed on silane-coated slides. For antigen retrieval, the slides were heated for 40 min at 97 °C in target Retrieval Solution (pH 9.0; Dako). They were then incubated at room temperature, first with Protein Block Serum-free Ready-to-Use solution (Dako) for 10 min, and then with an anti-ALK antibody (5A4, Abcam) for 30 min. To increase the sensitivity of detection, we included an incubation step of 15 min at room temperature with rabbit polyclonal antibodies to mouse immunoglobulin (Dako). The immune complexes were then detected with the dextran polymer reagent and an AutoStainer instrument (Dako).

2.2. Confirmation of EML4-ALK fusion gene by RT-PCR and FISH

We confirmed the existence of ALK fusion gene expression by fluorescence in situ hybridization (FISH) and/or by the reverse transcription-polymerase chain reaction (RT-PCR).

2.3. Fluorescence in situ hybridization (FISH)

An EML4-ALK fusion assay was performed [10–12]. Unstained sections were processed with a Histology FISH Accessory Kit (Dako), subjected to hybridization with fluorescence-labeled bacterial artificial chromosome clone probes for EML4 and ALK (self-produced probes; EML4: RP11-996L7, ALK: RP11-984I21 and RP11-62B19), stained with 4,6-diamidino-2-phenylindole, and examined with a fluorescence microscope (BX51; Olympus). The FISH positivity criteria specified "over 50% cancer cells" for EBUS-TBNA samples.

2.4. Reverse transcription-polymerase chain reaction (RT-PCR)

The multiplex PCR method proposed by the Japanese ALK lung cancer study group (ALCAS) was used to confirm the expression of ALK fusion gene [4–6].

Table 1
Characteristics of ALK fusion gene positive lung cancer patients.

Patient no	Sex	Age	SI	Histology	Variant	p Stage	Therapy	Recurrence	Distant meta	Survival (M)	Prognosis	ALK inhibitor case no
1	f	64	0	Ad: papillary	3	IIIA	Surgery	Positive	Bone, brain	21	Dead	
2	m	82	0	Ad: solid	2	IIIA	Surgery	Positive	Ascites	36	Alive	
3	f	68	0	Ad: papillary	3	IIIB	Surgery	Positive	Brain	34	Alive	
4	f	60	0	Ad: solid	3	IIIA	Surgery	Negative	None	29	Alive	
5	m	73	0	Ad: acinar	3	IA	Surgery	Negative	None	21	Alive	
6	m	66	0	Ad: papillary	KIF5B	IA	Surgery	Negative	None	15	Alive	
7	m	56	300	Ad: papillary	1	IA	Surgery	Negative	None	13	Alive	
8	m	46	0	Ad: acinar	5	IIIA	Surgery	Negative	None	22	Alive	
9	m	71	0	Ad: papillary	1	IIIA	Surgery	Negative		17	Alive	
10	f	73	0	Ad: acinar	1	IV	Surgery	Negative		14	Alive	
11	m	55	100	Ad: muc+	3	IV	BSC		Bone, brain	5	Dead	
12	m	48	0	Ad: muc+	1	IV	Chemo		Bone, brain	29	Dead	Case 1
13	f	49	0	Ad: muc+	3	IV	BSC		Bone, brain	15	Alive	Case 2
14	f	54	0	Ad: muc+	1	IV	Chemo		Bone, brain, pul	22	Alive	Case 3
15	f	64	0	Ad: acinar	3	IV	Chemo		Pul	2	Alive	

SI, smoking index; f, female; m, male; Ad, adenocarcinoma; muc+, mucin production; Distant meta, at the recurrence (surgery group) at the diagnosis (non-surgery group); pul, pulmonary metastasis; Case 1 was already reported by Nakajima et al. [16].

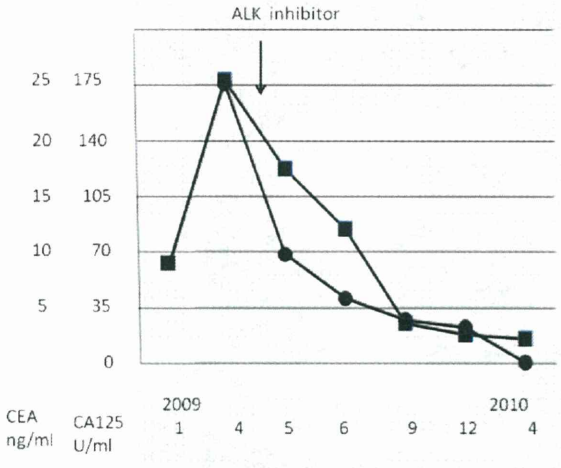

Fig. 1. Changes of tumor markers before and during the treatment with ALK inhibitor (Case 1) CEA (■), CA125 (●). Marked reduction of tumor markers was observed.

Total RNA was isolated from EBUS-TBNA or surgical samples using AllPrep DNA/RNA Mini Kit (Qiagen) and was reverse-transcribed into single strand cDNA using a High Capacity RNA-to-cDNA Kit (Applied Biosystems). To detect a fusion cDNA derived from EML4 or KIF5B and ALK, PCR analysis was performed with the AmpliTaq Gold PCR Master Mix (Applied Biosystems), the forward primers derived from EML4, EA-F-cDNA-S (5′-GTGCAGTGTTTAGCATTCTTGGGG-3′), EA-F-2-g-S (5′-AGCTACATCACACACCTTGACTGG-3′), EA-F-cDNA-v3-S-2 (5′-TACCAGTGCTGTCTCAATTGCAGG-3″) and EA-W-cDNA-in-S (5′-GCTTTCCCCGCAAGATGGACGG-3′) and the forward primers derived from KIF5B, KA-F-cDNA-S-e24 (5′-CAGCTGAGAGAGTGAAAGCTTTGG-3′), KA-F-cDNA-S-e17 (5′-GACAGTTGGAGGAATCTGTCGATG-3′), KA-F-cDNA-S-e11 (5′-ATCCTGCGGAACACTATTCAGTGG-3′), and KA-cDNA-S-e2 (5′-TCAAGCACATCTCAAGAGCAAGTG-3′) and the reverse primer derived from ALK, EA-F-cDNA-A (5′-TCTTGCCAGCAAAG-CAGTAGTTGG-3′). PCR products were purified from gel bands using QIAquick Gel Extraction Kit (Qiagen) and confirmed by direct sequencing analysis.

2.5. Enrolment of patients for the Clinical Trial A8081001

Informed consent was obtained from each patient to be enrolled for the study [10]. Eligibility criteria for the enrolment of ALK translocation positive patients into the ALK TKI PI Trial were as required by the Committee of Clinical Trials A8081001.

3. Results

There were 15 ALK fusion gene-positive cases which were screened immunohistochemically and confirmed by RT-PCR and FISH [14,15]. Eight patients were men and 7 women, of mean age

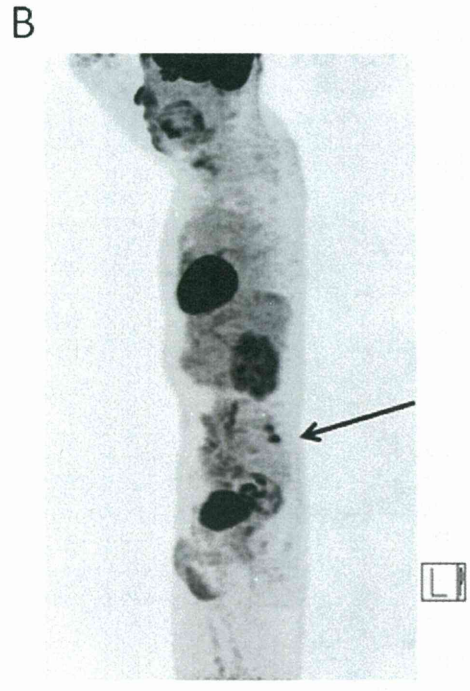

Fig. 2. FDG-PET scan of Case 1 performed at the same time (09/28/2009) as the previously reported Fig. 1D (Nakajima et al. [16]) shows bone metastasis of the left vertebral arch of L5 (arrow) in a sagittal view.

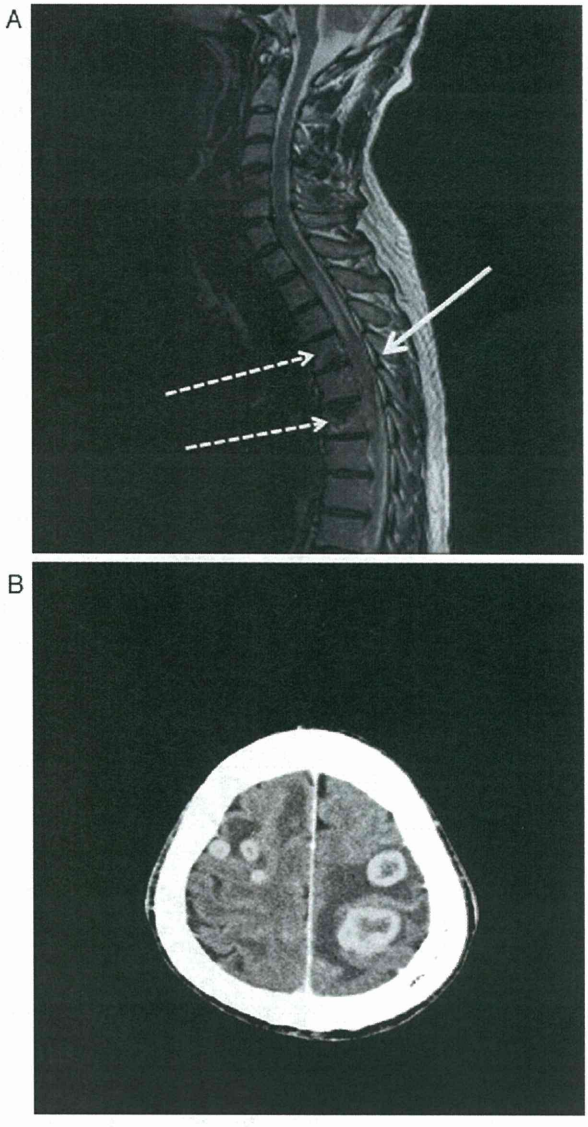

Fig. 3. MRI (Case 1) of the spinal cord on 04/05/2010 shows the metastases to the spinal cord (straight allow) and the spinal column (Th 4,6 dotted allow). B. CT scan (Case 1) of the brain on 04/05/2010 shows multiple brain metastases.

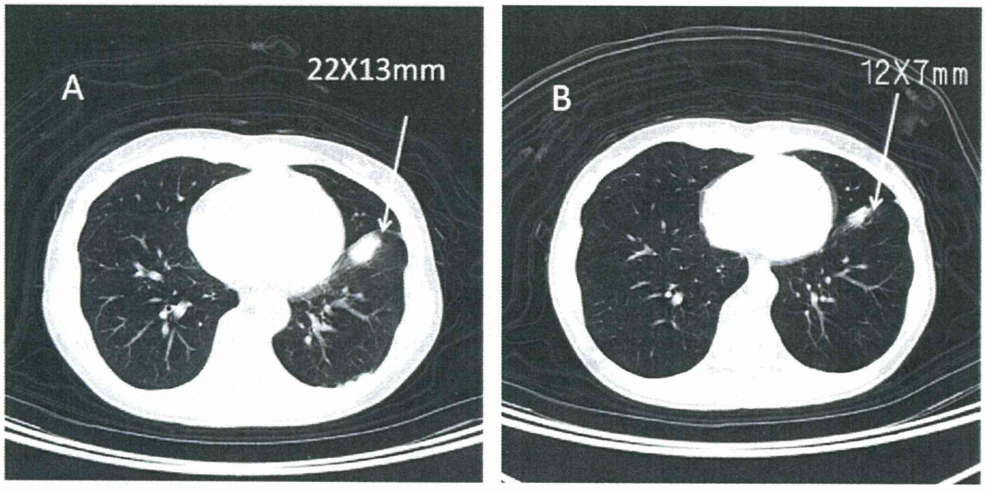

Fig. 4. CT scan (Case 2): A, 07/22/2009 (before ALK inhibitor) and B, 09/02/2009 (5 weeks after the initiation of the therapy). Left S8 tumor (arrow) decreased in size from 22X13 mm to 12X7 mm (PR).

61.9 years (range 48–82). Most were non-smokers, but 2 smoked lightly (Table 1). All tumors were adenocarcinomas with a papillary pattern predominant (5 cases), an acinar pattern predominant (3 cases), with mucin production (4 cases), etc. There were fourteen cases of fusion with EML4 and one KIF5B gene. There were 7 variant 3, 5 variant 1, and 1 each of variants 2 and 5. There were 3 stage IA, 5 stage IIIA, 1 stage IIIB and 6 stage IV cases. Ten cases were diagnosed after surgical resection, and 5, by tissue samples obtained with EBUS-TBNA. Ten cases underwent thoracotomy, 3 cases, chemotherapy, and 2 cases, only best supportive care. Of 5 cases diagnosed by EBUS-TBNA, 2 cases receiving chemotherapy and one receiving best supportive care were enrolled for the clinical trial. The mean age of the surgically treated group was 65.8 ± 10.1, and that of chemotherapy and BSC group was 54.0 ± 6.3. The difference was found by Student's t test to be statistically significant ($p < 0.05$), indicating that younger patients tend to have advanced cancer.

Out of 10 surgically treated cases, seven survived without a sign of recurrence, 3 had recurrence in both bone and brain tissue, and one died of bone and lymph node metastasis.

3.1. Case 1

Case 1 has already been reported in a case report (Nakajima et al.) [16] but without precise descriptions of the response to crizotinib, the adverse effects, the pattern of recurrence or the metastatic

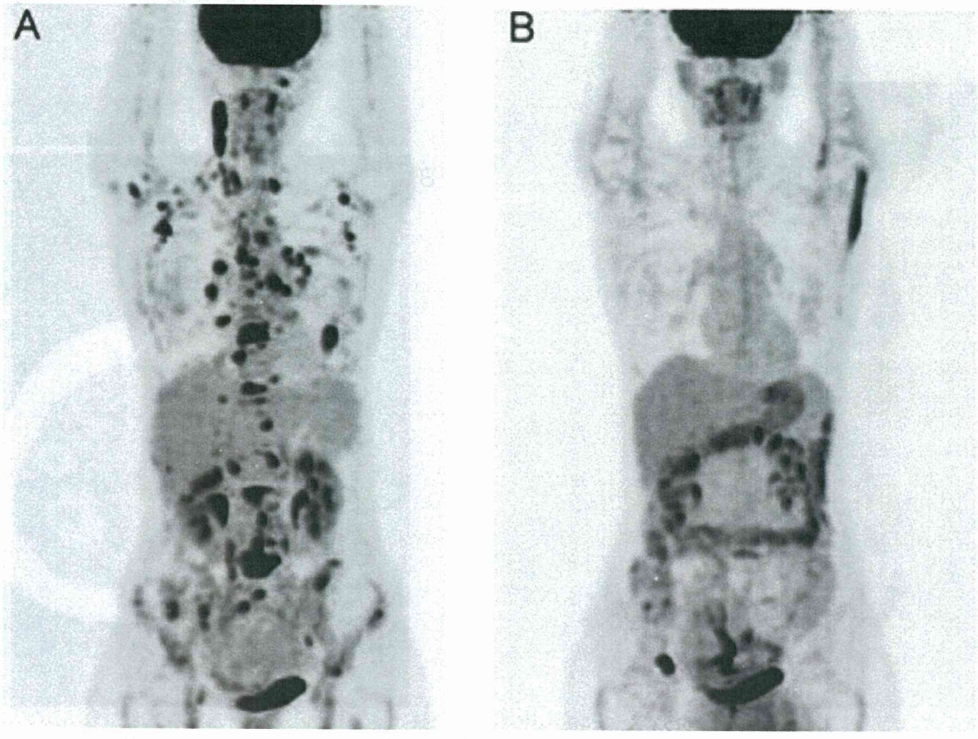

Fig. 5. FDG-PET scan (Case 2): A, 07/22/2009 (before ALK inhibitor) and B, 03/10/2010 FDG-PET scan shows marked reduction of accumulation in multiple bone and lymph node metastases 7 months after the initiation of the treatment.

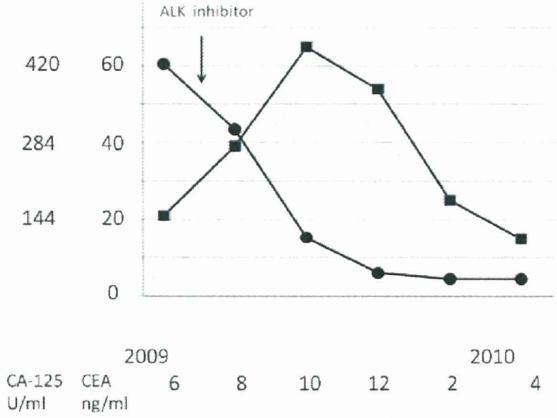

Fig. 6. Changes of tumor markers before and during the treatment with ALK inhibitor in case 2. CA125 (●) gradually decreased along with the treatment, but CEA (■) increased soon after the initiation of the therapy. The value of CEA then gradually decreased to 15.2 ng/ml in April 2010 (after 10 months).

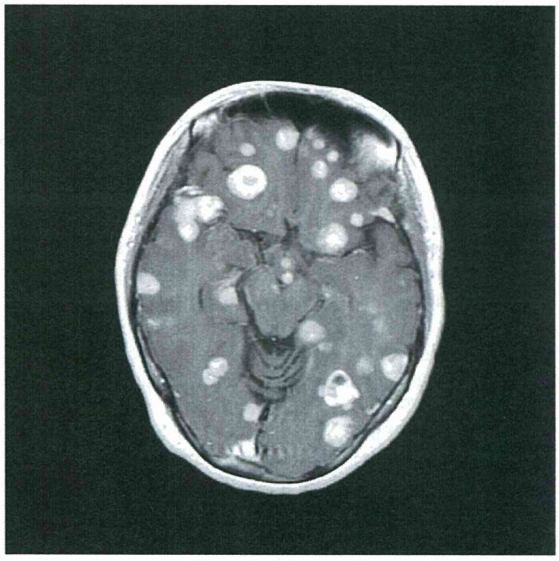

Fig. 7. Brain MRI of case 2 on 7/30/2010 showing multiple metastases.

tumor lesions. Such descriptions may contribute to a better understanding of the other cases, and so case 1 is described briefly below.

A 48-year-old non-smoking male patient had lung adenocarcinoma in the right lower lobe and multiple bone and lymph node metastases (T3N2M1 stage IV) at his first medical examination in November 2007. After several courses of chemotherapy, the patient was enrolled in a trial of crizotinib (PF02341066) from May 5th 2009 at Seoul National University, in which the drug was orally administered at 500 mg/day.

The effect of ALK inhibitor appeared rapidly. The patient's dyspnea improved within one week after drug administration. PS improved from 2 to 0 and a marked reduction in the tumor markers was observed (Fig. 1). Within 3 months after the start of therapy, almost all metastases disappeared except for those at the left vertebral arch of L5 (Fig. 2, arrow). The patient had severe adverse effects: diarrhea, nausea and persistence of light images started soon after the administration of the drug, but these gradually diminished over a 3-week period.

The control of the primary and metastatic tumors continued for 11 months until the patient visited Seoul University in April 2010, when he was hospitalized for paralysis of the lower extremities. MRI revealed spinal column (Th4-6) and spinal cord metastases (Fig. 3A). Soon after his hospitalization in our Cancer Center in April 2010, multiple brain metastases (Fig. 3B) were found, so the drug administration was stopped and he was transferred to a palliative care unit.

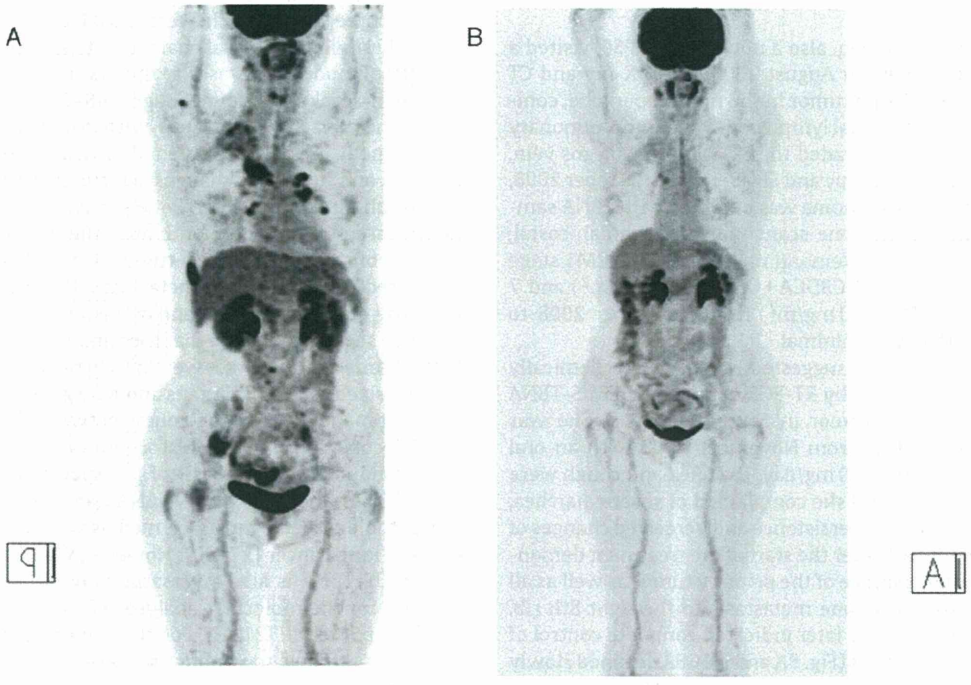

Fig. 8. FDG-PET scan: A, 09/08/2009 (before ALK inhibitor) and B, 07/05/2010 FDG-PET scan follow-up for 10 months indicated complete control of primary and distant metastases in case 3.

3.2. Case 2

A 49-year-old woman, a non-smoker with no history of illness, PS0, was introduced to the Orthopedics Department of our Center in April 2009 for back pain and multiple osteoplastic changes in the bones. Systematic examination revealed an abnormal shadow 22X13 mm in size in the left lower lobe (Fig. 4A). Bronchoscopy and a PET scan indicated left S8 adenocarcinoma with cervical, axial, mediastinal, hilar, pancreatic and retroperitoneal lymph node metastases, as well as cranial, thoracic (Th1-12), lumbar (L1-5), rib (1–12) pelvis, humerus, and femur metastases (Fig. 5A).

She refused any therapy except for best supportive care. One month after the examination, an additional immunohistochemical examination for EML4-ALK fusion protein was performed, and found to be positive. The presence of mRNA for EML4-ALK gene was also confirmed by RT-PCR and FISH from the mediastinal #4R lymph nodes obtained with EBUS-TBNA, which was performed 2 months later. EGFR mutation was negative, but the direct sequence of the EML4-ALK mRNA indicated that the translocation was variant 3 [9]. She decided to be enrolled to the crizotinib study (PF02341066) at a dosage of 500 mg/day at Seoul National University from July 2009.

She had nausea, diarrhea and light image persistence as in case 1, but her gastrointestinal symptoms were severer than those in case 1. Two weeks after the administration of ALK inhibitor, her back pain disappeared. A PET scan performed 5 weeks after the initiation of the therapy showed marked reduction of bone and lymph node metastases, and the primary tumor had decreased in size from 22X13 mm to 12X7 mm (Fig. 4A and B). Also, the SUV max dropped from 10.7 to 2.42. Changes of tumor markers were not parallel with the clinical course since the measured value of CA-125 dropped from 424 to 107 U/ml, but that of CEA increased from 21.5 to 65.4 ng/ml 4 months later. The value of CEA then gradually decreased to 15.2 ng/ml in April 2010 (10 months after that: Fig. 6). The PET scan conducted after 7 months indicated a partial response to multiple bone and lymph node metastases (Fig. 5B). The patient continued to take the drug until the end of July 2010, when brain metastases (Fig. 7) were found.

3.3. Case 3

A fifty-four-year-old woman, also a non-smoker, PS0, visited a doctor because of back pain in August 2008. Chest X-ray and CT scan showed an S3 59X22 mm tumor in the right upper lobe, combined with #4R, #2R mediastinal lymph nodes and intrapulmonary metastases. The tumor had invaded the SVC and the azygos vein. She had undergone bronchoscopy and EBUS-TBNA in October 2008. A diagnosis of lung adenocarcinoma was obtained with TBNA samples from #7 lymph nodes. Bone scans indicated cranial, costal, vertebral, scapular, pelvic and femoral metastases (T4N2M1 stage IV). She received 2 courses of CBDCA + GEM (1000 mg/m^2) and 7 courses of docetaxel (TXTL: 60 mg/m^2) from November 2008 to June 2009, but the effect was minimal.

EML4-ALK fusion gene was suggested immunohistochemically in August 2009 and confirmed by RT-PCR obtained by EBUS-TBNA samples from the primary tumor in September 2009. She was enrolled for the clinical trial from November 2009 with an oral administration of crizotinib 500 mg/day. Dyspnea and cough were alleviated within 2 weeks, and she complained of severe diarrhea, nausea, vomiting, light image persistence and perceived changes of taste. A PET scan one month after the start of the treatment demonstrated complete disappearance of the primary tumor as well as all the metastases except for a bone metastasis to the right 8th rib. A PET scan follow-up 8 months later indicated complete control of primary and metastatic tumors (Fig. 8A and B). CEA declined slowly from 1764 ng/ml to 79 ng/ml 6 months after the start of administration (Fig. 9). The patient had 12 brain metastases from 5 mm^3 to 309 mm^3 in volume and underwent gamma knife irradiation in August 2009, 2 months before the start of ALK inhibitor treatment. The irradiated field still showed little change for 5 months, but small new lesions appeared in the left occipital area 6 months after the start of the trial. Brain metastases grew very slowly, so we have maintained our observation until October 2010.

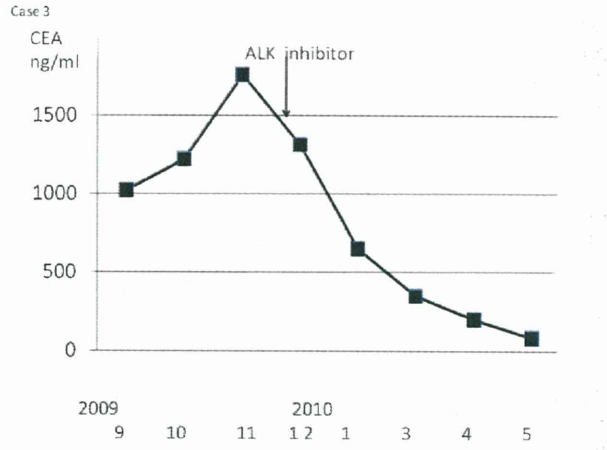

Fig. 9. CEA (■) declined slowly from 1764 ng/ml to 79 ng/ml 6 months after the start of the therapy in case 3.

4. Discussion

Above, we have reported the far-reaching effects of an ALK inhibitor on *EML4-ALK*-positive lung cancer patients. Soon after the administration of crizotinib, almost all metastases to bone and lymph nodes rapidly disappeared, followed by a marked reduction in the level of tumor markers in the sera. These observations clearly support the pivotal role of EML4-ALK oncokinase for the growth/survival of not only primary tumors but of the metastases. Such profound effects were rare among the patients when treated with conventional cytotoxic anticancer drugs.

The three cases which were enrolled for the study had surprisingly similar biological characteristics. They had multiple bone and lymph node metastases at the first medical examination, and were non-smokers at younger ages (48–54) who were resistant to chemotherapy. Adverse effects with crizotinib were also similar among them, including transient diarrhea, nausea, light image persistence, and subjective changes of taste. In addition, their response to ALK inhibitor was similar. Bone and lymph node metastases had disappeared within one month after the initiation of the therapy. The response of the primary tumor in case 2 was relatively slow compared with those of the metastases. The difference between the response of primary tumor and metastases to the ALK inhibitor in this case seems to indicate that the similar subclones of tumor cells in the primary tumors that were highly responsive to ALK inhibitor metastasized to distant organs and may give some explanation for the discrepancy in the time-course between CEA and CA125.

Molecular and immunohistochemical analyses in this cohort were conducted on the basis of the specimens obtained through EBUS-TBNA. Originally, EBUS-TBNA had been proposed useful for the pathological diagnosis of mediastinal involvement (N2 disease) of lung cancer [17–20]. However, we have already reported that EBUS-TBNA is also a versatile way of obtaining histological samples for the molecular analyses of cancer-related genes, such as *EGFR*, p53 et al. [21,22]. For those who have advanced NSCLC, it is often difficult to conduct surgery to obtain specimens from patients. Among such cases, however, EBUS-TBNA can usually be safely carried out to obtain specimens from enlarged mediastinal

lymph nodes or parathracheal tumors. We carried out EBUS-TBNA procedure for the reasons of its advantage in obtaining high quality core samples adequate for this purpose as well as its safety. We do not disregard the importance of TBB for the diagnosis of lung cancer; however, we needed histological samples to examine the immunohistochemistry and FISH for enrolment in a trial of crizotinib. Our experience with the three cases clearly demonstrates the importance and clinical relevance of obtaining such specimens for molecular analyses.

Although the initial effects of crizotinib are substantial in our cases, as well as in those reported by Bang et al. [10,11], such efficacy may not always last long. There was, for instance, development (case 1 and 2) and recurrence (case 3) of brain metastases while favorable control was maintained outside the brain. Given that the primary tumors and lymph node metastases were under control of crizotinib even at the appearance of brain metastases, the tumor cells outside the brain did not lose sensitivity to crizotinib. Relapses in the brain only may indicate either (i) subclones of the tumor acquired both the homing ability to the brain and resistance to crizotinib, or (ii) crizotinib may not penetrate the blood-brain barrier, leading to insufficient concentrations of crizotinib in the brain. It is thus highly important to examine in detail the molecular basis that would account for such acquired resistance to crizotinib, which may be secondary mutations within EML4-ALK itself or mutations/gene amplification of other genes, as demonstrated in the cases of acquired resistance of NSCLC to gefitinib/erlotinib [23–26].

Conflict of interest

None declared.

Acknowledgements

We are grateful to Dr. Yung-Jue Bang and the medical staff of Seoul National University Hospital for their support in the treatment of these patients. We also thank Mr. C.W.P. Reynolds of the Department of International Medical Communications, Tokyo Medical University, for his careful revision of the English of this manuscript.

References

[1] Janku F, Stewart DJ, Kurzrock R. Targeted therapy in non-small-cell lung cancer—Is it becoming a reality? Nat Rev Clin Oncol 2010 Jun 15;7(July (7)):401–14.
[2] Heinrich MC, Owzar K, Corless CL, et al. Correlation of kinase genotype and clinical outcome in the North American intergroup phase III trial of imatinib mesylate for treatment of advanced gastrointestinal stromal tumor: CALGB 150105 study by cancer and leukemia group B and southwest oncology group. J Clin Oncol 2008;26:5360–7.
[3] Mok TS, Wu YL, Yu CJ, et al. Randomized, placebo-controlled, phase II study of sequential erlotinib and chemotherapy as first-line treatment for advanced non-small-cell lung cancer. J Clin Oncol 2009;27:5080–7.
[4] Soda M, Choi YL, Enomoto M, et al. Identification of the transforming EML4-ALK fusion gene in non-small-cell lung cancer. Nature 2007;448:561–6.
[5] Mano H. Non-solid oncogenes in solid tumors: EML4-ALK fusion genes in lung cancer. Cancer Sci 2008;99:2349–55.
[6] Soda M, Takada S, Takeuchi K, et al. A mouse model for EML4-ALK-positive lung cancer. Proc Natl Acad Sci USA 2008;105:19893–7.
[7] Christensen JG, Zou HY, Arango ME, et al. Cytoreductive antitumor activity of PF-2341066, a novel inhibitor of anaplastic lymphoma kinase and c-Met, in experimental models of anaplastic large-cell lymphoma. Mol Cancer Ther 2007;6:3314–22.
[8] Koivunen JP, Mermel C, Zejnullahu K, et al. EML4-ALK fusion gene and efficacy of an ALK kinase inhibitor in lung cancer. Clin Cancer Res 2008;14: 4275–83.
[9] Kwak EL, Camidge DR, Clark J, et al. Clinical activity observed in a phase I dose escalation trial of an oral c-met and ALK inhibitor, PF-02341066. J Clin Oncol 2009;27:15s.
[10] Bang Y, Kwak EL, Shaw AT, et al. Clinical activity of the oral ALK inhibitor PF-02341066 in ALK-positive patients with non-small cell lung cancer (NSCLC). J Clin Oncol 2010;28:18s [suppl; abstr 3].
[11] Kwak EL, Bang YJ, Camidge DR, et al. Anaplastic lymphoma kinase inhibition in non-small-cell lung cancer. N Engl J Med 2010;363:1693–703.
[12] Takeuchi K, Choi YL, Togashi Y, et al. KIF5B-ALK, a novel fusion oncokinase identified by an immunohistochemistry-based diagnostic system for ALK-positive lung cancer. Clin Cancer Res 2009;15:3143–9.
[13] Inamura K, Takeuchi K, Togashi Y, et al. EML4-ALK lung cancers are characterized by rare other mutations, a TTF-1 cell lineage, an acinar histology, and young onset. Mod Pathol 2009;22:508–15.
[14] Shaw AT, Yeap BY, Mino-Kenudson M, et al. Clinical features and outcome of patients with non-small-cell lung cancer who harbor EML4-ALK. J Clin Oncol 2009;27(September (26)):4247–53.
[15] Takahashi T, Snooze M, Kobayashi M, et al. Clinicopathologic features of non-small-cell lung cancer with EML4-ALK fusion gene. Ann Surg Oncol 2010;17(March (3)):889–97.
[16] Nakajima T, Kimura H, Takeuchi K, et al. Treatment of lung cancer with an ALK inhibitor after EML4-ALK fusion gene detection using endobronchial ultrasound-guided transbronchial needle aspiration. J Thorac Oncol 2010;5:2041–3.
[17] Yasufuku K, Chiyo M, Koh E, et al. Endobronchial ultrasound guided transbronchial needle aspiration for staging of lung cancer. Lung Cancer 2005;50:347–54.
[18] Yasufuku K, Chiyo M, Sekine Y, et al. Real-time endobronchial ultrasound-guided transbronchial needle aspiration of mediastinal and hilar lymph nodes. Chest 2004;126:122–8.
[19] Herth FJ, Eberhardt R, Vilmann P, Krasnik M, Ernst A. Real-time endobronchial ultrasound guided transbronchial needle aspiration for sampling mediastinal lymph nodes. Thorax 2006;61:795–8.
[20] Herth FJ, Ernst A, Eberhardt R, Vilmann P, Dienemann H, Krasnik M. Endobronchial ultrasound-guided transbronchial needle aspiration of lymph nodes in the radiologically normal mediastinum. Eur Respir J 2006;28: 910–4.
[21] Nakajima T, Yasufuku K, Suzuki M, et al. Assessment of epidermal growth factor receptor mutation by endobronchial ultrasound-guided transbronchial needle aspiration. Chest 2007;132:597–602.
[22] Mohamed S, Yasufuku K, Nakajima T, et al. Analysis of cell cycle-related proteins in mediastinal lymph nodes of patients with N2-NSCLC obtained by EBUS-TBNA: relevance to chemotherapy response. Thorax 2008;63:642–7.
[23] Kobayashi S, Boggon TJ, Dayaram T, et al. EGFR mutation and resistance of non-small-cell lung cancer to gefitinib. N Engl J Med 2005;352:786–92.
[24] Lu L, Ghose AK, Quail MR, et al. ALK mutants in the kinase domain exhibit altered kinase activity and differential sensitivity to small molecule ALK inhibitors. Biochemistry 2009;48:3600–9.
[25] Gazdar AF. Activating and resistance mutations of *EGFR* in non-small-cell lung cancer: role in clinical response to EGFR tyrosine kinase inhibitors. Oncogene 2009;28:S24–31.
[26] Choi YL, Soda M, Yamashita Y, et al. EML4-ALK mutations in lung cancer that confer resistance to ALK inhibitors. N Engl J Med 2010;363:1734–9.

OPEN ACCESS Freely available online

PLoS one

Oncogenic LMO3 Collaborates with HEN2 to Enhance Neuroblastoma Cell Growth through Transactivation of *Mash1*

Eriko Isogai[1,2], Miki Ohira[2], Toshinori Ozaki[3], Shigeyuki Oba[4], Yohko Nakamura[1], Akira Nakagawara[1]*

1 Division of Biochemistry and Innovative Cancer Therapeutics, Chiba Cancer Center Research Institute, Chuoh-ku, Chiba, Japan, **2** Laboratory of Cancer Genomics, Chiba Cancer Center Research Institute, Chuoh-ku, Chiba, Japan, **3** Laboratory of Anti-Tumor Research, Chiba Cancer Center Research Institute, Chuoh-ku, Chiba, Japan, **4** Integrated Systems Biology Laboratory, Department of Systems Science, Graduate School of Informatics, Kyoto University, Gokasho, Uji, Kyoto, Japan

Abstract

Expression of *Mash1* is dysregulated in human neuroblastoma. We have also reported that LMO3 (LIM-only protein 3) has an oncogenic potential in collaboration with neuronal transcription factor HEN2 in neuroblastoma. However, the precise molecular mechanisms of its transcriptional regulation remain elusive. Here we found that LMO3 forms a complex with HEN2 and acts as an upstream mediator for transcription of *Mash1* in neuroblastoma. The high levels of *LMO3* or *Mash1* mRNA expression were significantly associated with poor prognosis in 100 primary neuroblastomas. The up-regulation of *Mash1* remarkably accelerated the proliferation of SH-SY5Y neuroblastoma cells, while siRNA-mediated knockdown of *LMO3* induced inhibition of growth of SH-SY5Y cells in association with a significant down-regulation of *Mash1*. Additionally, overexpression of both LMO3 and HEN2 induced expression of *Mash1*, suggesting that they might function as a transcriptional activator for *Mash1*. Luciferase reporter assay demonstrated that the co-expression of LMO3 and HEN2 attenuates HES1 (a negative regulator for *Mash1*)-dependent reduction of luciferase activity driven by the *Mash1* promoter. Chromatin immunoprecipitation assay revealed that LMO3 and HEN2 reduce the amount of HES1 recruited onto putative HES1-binding sites and E-box within the *Mash1* promoter. Furthermore, both LMO3 and HEN2 are physically associated with HES1 by immunoprecipitation assay. Thus, our present results suggest that a transcriptional complex of LMO3 and HEN2 may contribute to the genesis and malignant phenotype of neuroblastoma by inhibiting HES1 which suppresses the transactivation of *Mash1*.

Citation: Isogai E, Ohira M, Ozaki T, Oba S, Nakamura Y, et al. (2011) Oncogenic LMO3 Collaborates with HEN2 to Enhance Neuroblastoma Cell Growth through Transactivation of *Mash1*. PLoS ONE 6(5): e19297. doi:10.1371/journal.pone.0019297

Editor: Laszlo Tora, Institute of Genetics and Molecular and Cellular Biology, France

Received December 21, 2010; **Accepted** March 31, 2011; **Published** May 5, 2011

Funding: This work was supported in part by a Grant-in-Aid from the Ministry of Health, Labour and Welfare for the Third Term Comprehensive Control Research for Cancer; a Grant-in-Aid for Scientific Research on Priority Areas from the Ministry of Education, Culture, Sports, Science and Technology, Japan; and a Grant-in-Aid for Scientific Research from Japan Society for the Promotion of Science. The funders had no role in study design, data collection and analysis, decision to publish, or preparation of the manuscript.

Competing Interests: The authors have declared that no competing interests exist.

* E-mail: akiranak@chiba-cc.jp

Introduction

Neuroblastoma is one of the typical childhood cancers and is originated from sympathetic cell lineage of the neural crest [1,2]. Since the tumor never occurs from the other lineages of the neural crest, the oncogenic events to cause neuroblastoma might be strictly regulated in a lineage-specific manner [1,2].

LIM-only protein (LMO) family is composed of four members, LMO1, LMO2, LMO3 and LMO4. Although LMO proteins lack a DNA-binding activity, accumulating evidence suggest that LMO proteins are involved in transcriptional regulation of specific target genes in collaboration with other transcription factors [3]. Genetic analyses demonstrated that LMO1 and LMO2 contribute to the genesis of immature and aggressive T-cell leukemia [4], whereas LMO4 was implicated in development of breast cancer [5,6]. Previously, we reported that *LMO3* is expressed at significantly high levels in human unfavorable neuroblastomas relative to favorable ones, and has an oncogenic potential in neuroblastoma [7]. LMO3 formed a complex with neuronal-specific basic helix-loop-helix (bHLH) transcription factor HEN2, which was also expressed at higher levels in unfavorable neuroblastoma than favorable one, raising a possibility that LMO3 may form a complex with HEN2 and play an important role in genesis and development of neuroblastoma through transcriptional regulation of as yet unidentified target gene(s).

A proneural bHLH transcription factor termed Mash1 plays a critical role in development of sympathetic neuron and is highly expressed in neuroblastoma [8,9]. However, its possible contribution to development of neuroblastoma remains elusive. A bHLH protein termed HES1 acts as a negative regulator for *Mash1* [10]. Intriguingly, studies in *Drosophila* demonstrated that expression levels of *achaete-scute*, a *Drosophila* homolog of *Mash1*, are remarkably induced by a transcriptional complex composed of *Drosophila* homolog of LMO (dLMO) and bHLH proteins [11,12].

In this study, we examined whether there could exist functional relationship between LMO3/HEN2 and Mash1 in neuroblastoma, and found that LMO3/HEN2 attenuates HES1 function and enhances transactivation of *Mash1*, leading to aggressive phenotype of neuroblastoma.

Results

High levels of *Mash1* expression is associated with poor outcome of neuroblastoma

Mash1 is constitutively expressed at high levels in neuroblastoma cell lines and primary neuroblastoma tumors [9,13], however, its prognostic significance remained elusive. On the other hand, expression of *LMO3* was significantly associated with poor outcome of the patients [7]. To verify whether a significant relationship could be observed between expression of *LMO3* and that of *Mash1* in primary neuroblastomas, we quantitatively measured the expression levels of *LMO3* and *Mash1* mRNA in 100 primary tumors by using a quantitative real-time RT-PCR. The student's t-test showed that high expression of *LMO3* was significantly associated with ≥1 year of age ($p = 0.036$), low expression of *TrkA* ($p = 0.003$) and *MYCN* amplification ($p = 0.04$), but not with the tumor stage ($p = 0.17$), tumor origin ($p = 0.083$) and Shimada classification ($p = 0.082$). High expression of *Mash1* was significantly associated with advanced tumor stage ($p = 0.004$) but not with age ($p = 0.81$), *TrkA* expression ($p = 0.4$), *MYCN* copy number ($p = 0.11$), tumor origin ($p = 0.2$) and Shimada classification ($p = 0.45$) (Table S1). No significant relationship was observed between *LMO3* and *Mash1* mRNA expression levels (the Pearson correlation coefficient was 0.27). Kaplan-Meier survival curves indicated that high expression of *LMO3* as well as that of *Mash1* were significantly associated with poor prognosis (log-rank test, $p = 0.006$ and $p = 0.037$, respectively; Figure 1). The univariate analysis according to the Cox proportional hazard model also indicated that the expression levels of *Mash1* and those of *LMO3* were significantly associated with poor outcome of the patients ($p = 0.048$ and $p = 0.012$, respectively; Table S2). The multivariate Cox proportional hazard model analysis showed that the expression of *Mash1* was significantly independent prognostic factor from *LMO3* expression and age, marginally from *MYCN* copy number and origin, but not from the disease stage, and that the expression of *LMO3* was significantly independent prognostic factor from *Mash1* expression, age, the disease stage and origin, but not from *MYCN* copy number (Table S2). Thus, the results obtained from the primary neuroblastomas suggested that both high mRNA expression of *LMO3* and *Mash1* were strongly associated with poor prognoses of the patients with neuroblastoma but the way of contribution of those seemed to be rather independent.

Mash1 mediates growth promotion of neuroblastoma cells

Since *Mash1* is highly expressed in primary neuroblastoma [9] and its higher expression was significantly correlated with poor prognosis of the patient with neuroblastoma, we then investigated a possible contribution of Mash1 to neuroblastoma cell growth. For this purpose, we established three stable *Mash1* infectants derived from the parental SH-SY5Y neuroblastoma cells expressing exogenous Mash1 (M-1, M-2 and M-3) and two control vector alone infectants (V-1 and V-2) by retrovirus-mediated gene transfer (Figure 2A). As shown in Figure 2B, constitutive expression of *Mash1* in SH-SY5Y cells resulted in a remarkable increase in their growth rate as compared with the control infectants, suggesting that Mash1 is involved in regulation of neuroblastoma cell growth.

As described previously [7], LMO3 has an oncogenic potential in collaboration with HEN2 in neuroblastoma cells. We then asked whether or not LMO3 is involved in the Mash1-mediated enhancement of cell growth. As shown in Figure 2C, siRNA-mediated knockdown of *LMO3* in SH-SY5Y cells was significantly associated with a down-regulation of *Mash1*. Additionally, LMO3-knocked down SH-SY5Y cells showed a slower growth rate than the control SH-SY5Y cells (Figure 2D), which might be at least in part due to reduction of *Mash1*. We conducted the same experiments by using another cell line SK-N-BE and obtained the similar results (Figure S1A and B). We then hypothesized that *Mash1* could be one of transcriptional targets of LMO3/HEN2 complex.

LMO3/HEN2 mediate transcriptional induction of *Mash1*

To address whether *Mash1* transcription could be induced by LMO3/HEN2, SH-SY5Y cells were infected with the indicated combinations of recombinant adenoviruses encoding HA-LMO3 or FLAG-HEN2, and the expression levels of *Mash1* were examined by semi-quantitative RT-PCR. Time course experiments demonstrated that *Mash1* is readily detectable in cells expressing HA-LMO3 alone or in cells co-expressing with HA-LMO3 and FLAG-HEN2 at 48 h after infection

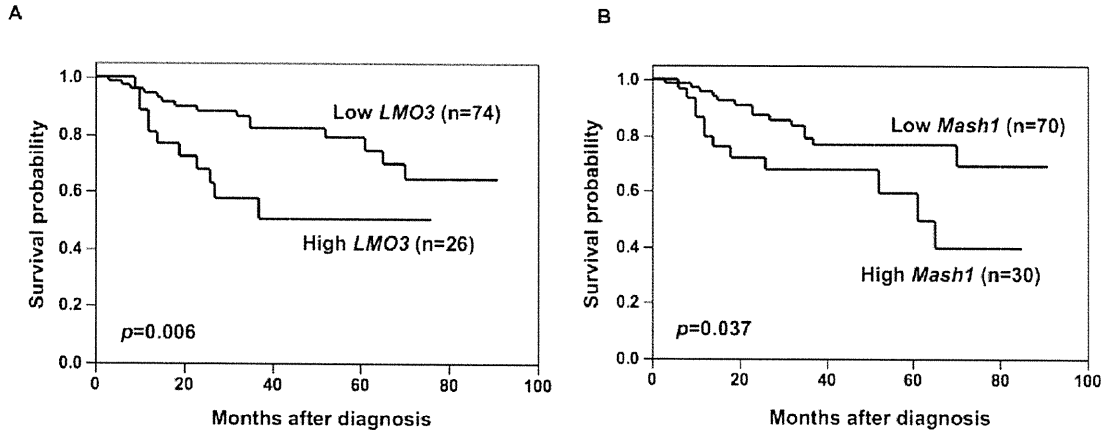

Figure 1. Kaplan-Meier survival curves of patients with neuroblastomas based on high or low expression of *LMO3* (A) or *Mash1* (B). Kaplan-Meier survival curves (n = 100) in relation to the expression levels of *LMO3* or *Mash1* (average cutoff). The patients with high expression of *LMO3* or *Mash1* represented significantly poor prognosis than those with its low expression.
doi:10.1371/journal.pone.0019297.g001

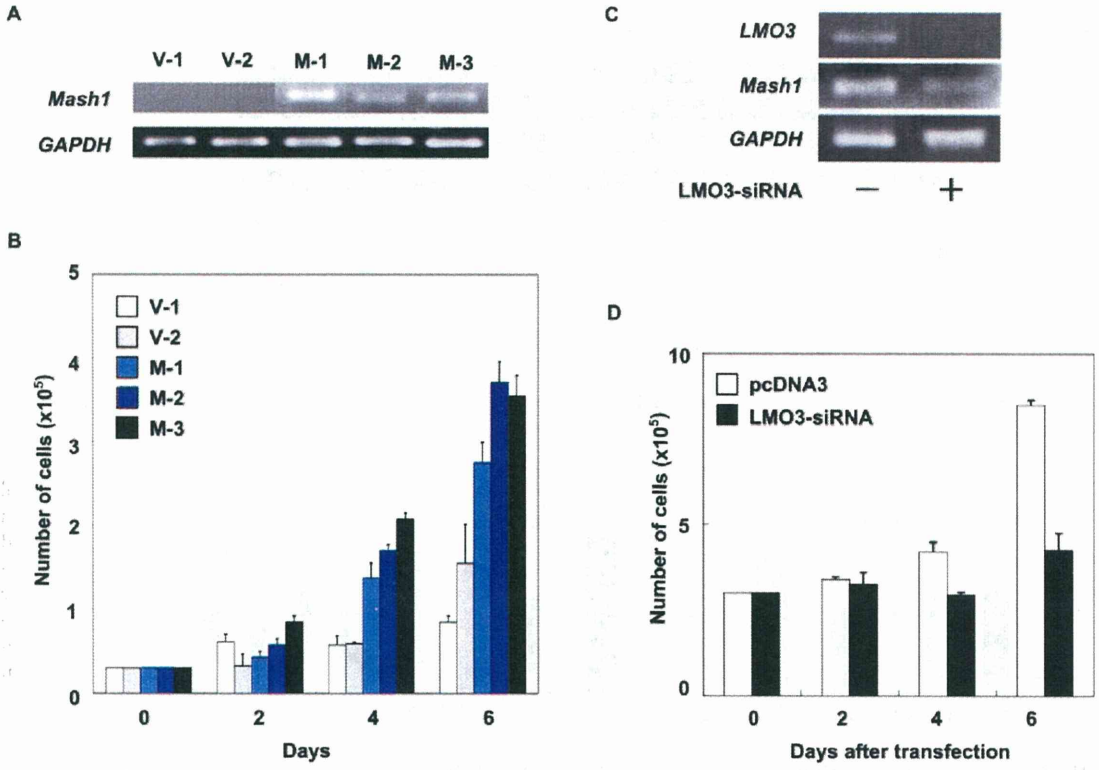

Figure 2. Mash1-mediated growth promotion of neuroblastoma cells. (A) Enforced expression of *Mash1*. Neuroblastoma SH-SY5Y cells were infected with empty retrovirus or with retrovirus encoding Mash1 and established two control infectants (V-1 and V-2) and three infectants expressing *Mash1* (M-1, M-2 and M-3). Total RNA was extracted from the indicated cell clones and subjected to RT-PCR to examine expression levels of *Mash1*. *GAPDH* was used as an internal control. (B) Mash1-mediated growth promotion. The indicated infectants were seeded at a density of 3×10^4/cell culture dish and allowed to attach overnight. At the indicated time periods, number of viable cells was measured. (C) siRNA-mediated knockdown of LMO3. SH-SY5Y cells were transfected with empty plasmid (4 μg) or with expression plasmid for siRNA targeting LMO3 (4 μg). Forty-eight hours after transfection, total RNA was prepared and analyzed for expression levels of *LMO3* and *Mash1* by RT-PCR. (D) Decreased growth rate in LMO3-knocked down cells. SH-SY5Y cells (3×10^5 cells/cell culture dish) were transfected as in (C). Forty-eight hours after transfection, cells were transferred into fresh medium. At the indicated time points, number of viable cells was measured.
doi:10.1371/journal.pone.0019297.g002

(Figure 3A). Seventy-two hours after infection, co-expression of HA-LMO3 and FLAG-HEN2 led to a significant induction of *Mash1*. The induction of *Mash1* was also observed in SK-N-BE cells transfected with expression vector HA-LMO3 alone or HA-LMO3 and FLAG-HEN2 at 72 h after transfection (Figure S1C). To further confirm these observations, we generated a luciferase reporter construct carrying human *Mash1* promoter (pluc-Mash1). As shown in Figure 3B, the 5′-upstream region of *Mash1* gene contains three putative HES1-binding sites and one E-box. In both SH-SY5Y cells and SK-N-BE cells, siRNA-mediated knockdown of human *LMO3* reduced promoter activity of *Mash1* in a dose-dependent manner (Figure 3C and Figure S1D). For luciferase reporter assay without siRNA for human LMO3, we used mouse neuroblastoma Neuro2a cells which displayed higher transfection efficiency than human neuroblastoma cells as examined by GFP staining (data not shown). Consistent with the above expression studies, LMO3 enhanced luciferase activity driven by *Mash1* promoter (Figure 3D). Furthermore, we examined the effect of HEN2 on *Mash1* promoter activity in Neuro2a cells, showing that HEN2 itself inhibited *Mash1* promoter activity (Figure 3E). Intriguingly, however, LMO3 interfered with HEN2 function, resulting in up-regulation of *Mash1* transcription (Figure 3F). Thus, it is likely that the LMO3 complex including HEN2 and HES1 regulates transcription of *Mash1*. The mRNA expression pattern of *LMO3*, *HEN2*, *Mash1* and *HES1*, a negative regulator of *Mash1* transcription, in neuroblastoma cell lines is shown in Figure S2.

LMO3/HEN2 attenuates HES1-dependent down-regulation of *Mash1*

As reported previously [10], HES1 is one of the negative regulators for *Mash1*. In accordance with the previous observations, enforced expression of HES1 dramatically reduced luciferase activity driven by *Mash1* promoter (Figure 4A). The inhibitory effect of HES1 on *Mash1* promoter was stronger than that of HEN2. To investigate the relationships between HES1 and LMO3/HEN2 in transcriptional regulation of *Mash1*, we examined effects of HEN2 and LMO3 on HES1-dependent down-regulation of *Mash1* (Figure 4B). The HES1-dependent inhibition of *Mash1* promoter activity was attenuated by co-expression with FLAG-HEN2 alone or with co-expression with FLAG-HEN2 plus HA-LMO3. Inhibitory effects of FLAG-HEN2 plus HA-LMO3 on HES1 were larger than that of FLAG-HEN2 alone, suggesting that LMO3/HEN2 complex plays a critical role in regulation of *Mash1* transcription by neutralizing the inhibitory effect of HES1.

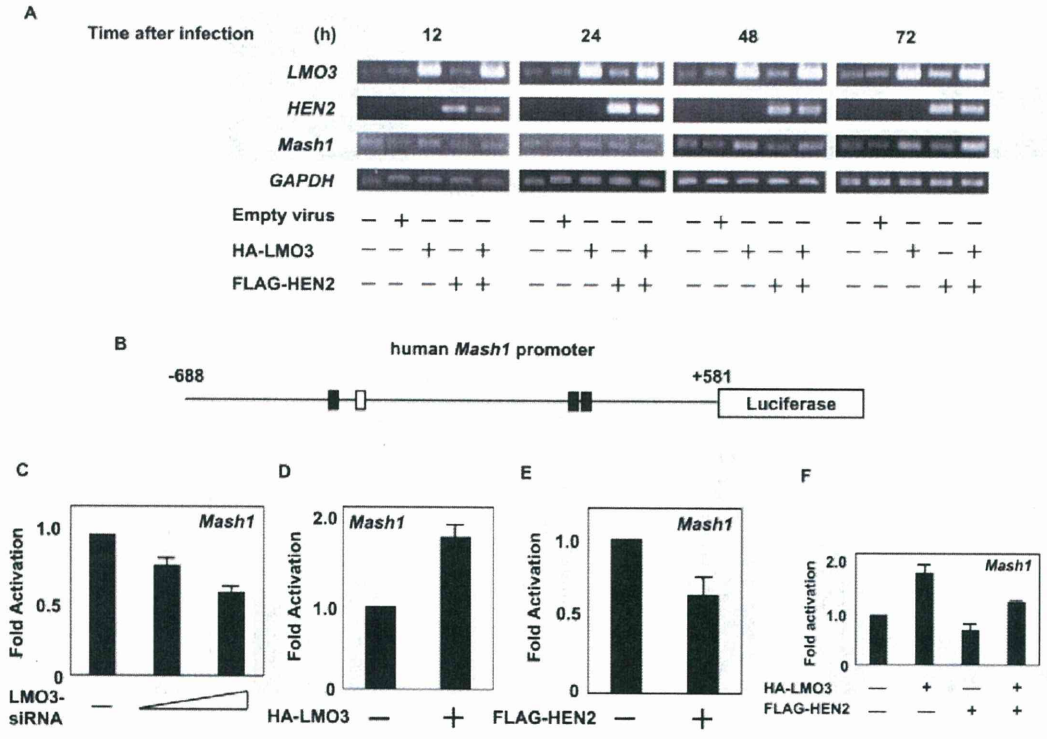

Figure 3. LMO3/HEN2-mediated transcriptional induction of *Mash1*. (A) RT-PCR. SH-SY5Y cells were infected with empty adenovirus or with the indicated combinations of recombinant adenovirus encoding HA-LMO3 or FLAG-HEN2. At the indicated time points after infection, total RNA was analyzed for expression levels of *LMO3*, *HEN2* and *Mash1* by RT-PCR. *GAPDH* was used as an internal control. (B) Schematic drawing of human *Mash1* promoter. Nucleotide positions were indicated relative to transcriptional initiation site (+1). The putative HES1-binding sites and E-box were depicted by filled and open boxes, respectively. This genomic fragment was subcloned into appropriate restriction sites of pGL3-Basic Vector to give pluc-hMash1. (C) siRNA-mediated knockdown of LMO3 reduces the promoter activity of *Mash1*. SH-SY5Y cells were co-transfected with constant amount of pluc-Mash1 (100 ng) and pRL-CMV (0.2 ng) in the presence or absence of increasing amounts of expression plasmid for siRNA against human LMO3 (100 or 400 ng). Forty-eight hours after transfection, cells were lysed and their luciferase activities were measured. (D) LMO3 transactivates *Mash1* promoter. Mouse neuroblastoma Neuro2a cells (1×10^5 cells/24-well plate) were co-transfected with constant amount of pluc-hMash1 (100 ng) and pRL-CMV (0.2 ng) together with or without expression plasmid for HA-LMO3 (150 ng). Forty-eight hours after transfection, cells were lysed and their luciferase activities were measured. (E) HEN2 inhibits *Mash1* promoter activity. Luciferase activities were measured in Neuro2a cells with or without FLAG-HEN2 (100 ng). (F) LMO3 interferes with negative effect of HEN2 on Mash1 transcription in Neuro2a cells. Luciferase activities were measured in Neuro2a cells transfected with HA-LMO3 (150 ng), FLAG-HEN2 (100 ng) or both of them.
doi:10.1371/journal.pone.0019297.g003

To ask about mechanistic insights into understanding how LMO3 and/or HEN2 could attenuate the inhibitory effects of HES1 on *Mash1* expression, we performed chromatin immunoprecipitation (ChIP) assay. Similar to human *Mash1* promoter, mouse *Mash1* promoter also contains three putative HES1-binding sites and one E-box (Figure 4C). Neuro2a cells were transfected with constant amount of empty plasmid or with expression plasmid for Myc-HES1 together with or without increasing amounts of FLAG-HEN2 expression plasmid. Forty-eight hours after transfection, cross-linked chromatin was prepared and subjected to ChIP assay. As shown in Figure 4D, the anti-Myc tag immunoprecipitates contained genomic fragments including putative HES1-binding sites as well as E-box. The amounts of Myc-HES1 recruited onto HES1-binding sites and E-box significantly decreased in the presence of FLAG-HEN2 in a dose-dependent manner. Additionally, the anti-FLAG immunoprecipitates contained genomic fragments including putative HES1-binding sites and E-box in the absence of exogenous HES1. Co-expression of FLAG-HEN2 and Myc-HES1 inhibited recruitment of FLAG-HEN2 onto putative HES1-binding sites and E-box, however, its inhibition was efficiently abrogated by increasing amounts of FLAG-HEN2. These results suggest that HEN2 might compete with HES1 in binding to putative HES1-binding sites and E-box, and thereby inducing the expression of *Mash1*.

HEN2 Interacts with HES1 in cells

To examine whether HEN2 could interact with HES1 in cells, we performed immunoprecipitation experiments. Cell lysates prepared from Neuro2a cells co-transfected with the indicated combinations of expression plasmids were subjected to immunoprecipitation. As clearly shown in Figure 5A, HES1 was co-immunoprecipitated with FLAG-HEN2. Consistent with these results, reciprocal experiments showed that the anti-Myc tag immunoprecipitates contain FLAG-HEN2. *In vitro* pull-down assay demonstrated that radio-labeled FLAG-HEN2 is co-immunoprecipitated with Myc-HES1 (Figure 5B). Additional immunoprecipitation experiments demonstrated that LMO3 also forms a stable complex with HES1 (Figure 6A). We have previously showed that LMO3 forms a stable complex with HEN2 [7]. To investigate the effect of LMO3 on binding of HEN2 and HES1 to putative HES1-binding sites and E-box,

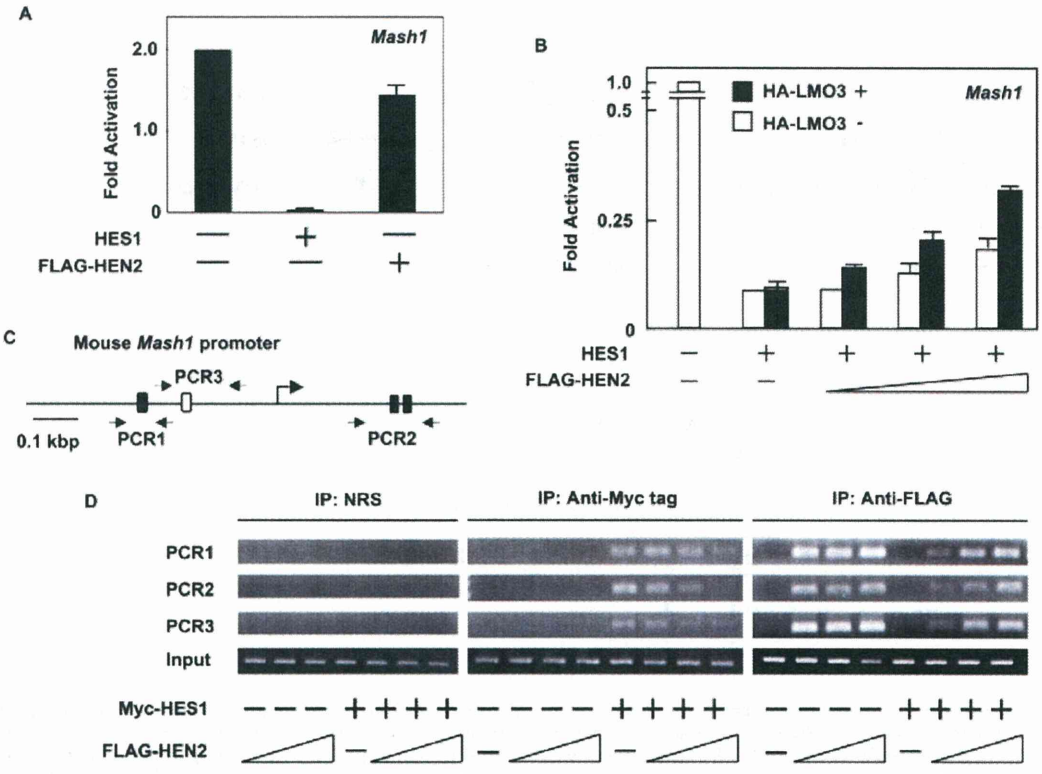

Figure 4. LMO3/HEN2 attenuates HES1-dependent down-regulation of *Mash1*. (A) Luciferase reporter assay. Neuro2a cells were co-transfected with constant amount of pluc-hMash1 (100 ng), pRL-CMV (0.2 ng) and expression plasmid for HES1 (50 ng) or HEN2 (50 ng). Forty-eight hours after transfection, cells were lysed and their luciferase activities were examined. (B) Luciferase reporter assay. Neuro2a cells were co-transfected with constant amount of pluc-hMash1 (100 ng), pRL-CMV (0.2 ng) and expression plasmid for HES1 (5 ng) in the presence or absence of expression plasmid for HA-LMO3 (150 ng) together with or without increasing amounts of FLAG-HEN2 expression plasmid (100, 200 or 300 ng). Forty-eight hours after transfection, cells were lysed and their luciferase activities were examined. (C) Schematic representation of mouse *Mash1* promoter. The canonical HES1-binding sites and E-box were indicated by filled and open boxes, respectively. The positions of primer sets used for chromatin immunoprecipitation (ChIP) assays were also indicated. (D) ChIP assay. Cross-linked chromatin prepared from Neuro2a cells transfected with the indicated combinations of expression plasmids was sonicated and immunoprecipitated with normal rabbit serum (NRS), polyclonal anti-Myc tag or with polyclonal anti-FLAG antibody. The genomic DNA was purified from the immunoprecipitates and amplified by PCR.
doi:10.1371/journal.pone.0019297.g004

Neuro2a cells were transfected with Myc-HES1 or FLAG-HEN2 together with or without HA-LMO3 expression plasmid and subjected to ChIP assay. As shown in Figure 6B, the immunoprecipitates using anti-Myc tag or anti-FLAG tag antibody contained genomic fragments including putative HES1-binding sites as well as E-box. The amount of Myc-HES1 recruited onto HES1-binding sites and E-box decreased in the presence of HA-LMO3. On the other hand, the amount of FLAG-HEN2 recruited onto HES1-binding sites and E-box increased in the presence of HA-LMO3. As shown in Figure 3F, LMO3 interferes with inhibitory effect of HEN2 on Mash1 expression. These suggest that LMO3 may additively interfere with the inhibitory effect of HES1 on *Mash1* expression by promoting binding of HEN2 to HES1-binding sites and E-box. Collectively, it is conceivable that LMO3/HEN2 reduces the inhibitory effect of HES1 on *Mash1* expression through binding to HES1 and thereby blocking its recruitment onto putative HES1-binding sites and E-box (Figure 7 and Figure S3).

Discussion

In this study, we found that *Mash1* is one of transcriptional targets of LMO3/HEN2 transcriptional complex, and its protein product may play an important role in regulation of neuroblastoma cell growth. As described previously [14], *HEN1* as well as its closely related gene *HEN2* encodes bHLH-type transcription factor, which might recognize E-box (5′-CACGTG-3′). On the other hand, HES1 has an intrinsic transcriptional repressor activity [10]. Based on our present results, adenovirus-mediated expression of LMO3/HEN2 significantly induced *Mash1*, and HES1-mediated down-regulation of *Mash1* promoter activity was recovered by co-expression of LMO3 and HEN2. Our ChIP analyses indicated that HES1 binds to HES1-recognition sites and E-box within *Mash1* promoter in the absence of HEN2, whereas HEN2 efficiently inhibits the recruitment of HES1 onto HES1-binding sites and E-box within *Mash1* promoter, suggesting that HES1 occupies HES1-binding sites and E-box to inhibit the promoter activity of *Mash1*. On the other hand, HEN2 formed a complex with HES1 and reduced the amounts of HES1 recruited onto HES1-binding sites as well as E-box to increase the promoter activity of *Mash1* in collaboration with LMO3. Thus, it is likely that the balance between intracellular amounts of HES1 and LMO3/HEN2 might determine expression levels of *Mash1*, and thereby regulating neuroblastoma cell growth.

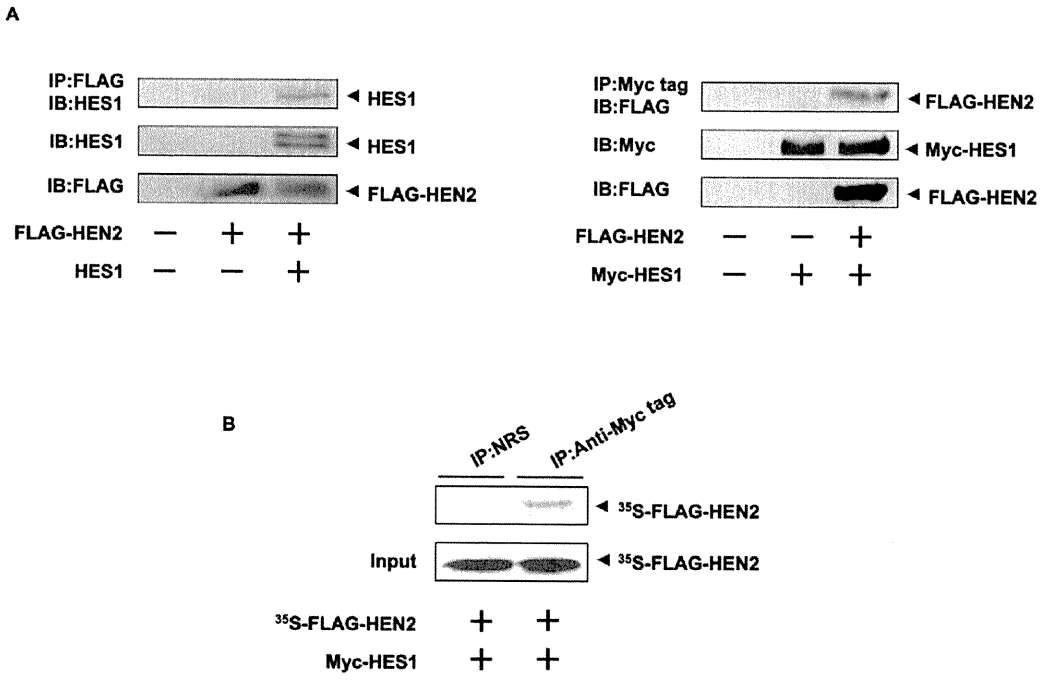

Figure 5. Interaction between HEN2 and HES1 in cells. (A) Neuro2a cells were co-transfected with the indicated combinations of expression plasmids. Forty-eight hours after transfection, cells were lysed and immunoprecipitated with anti-FLAG (left panel) or with anti-Myc tag antibody (right panel) and the immunoprecipitates were analyzed by immunoblotting with anti-HES1 or with anti-FLAG antibody, respectively. Aliquots of cell lysates were subjected to immunoblotting with anti-HES1, anti-FLAG or with anti-Myc tag antibody. (B) *In vitro* pull-down assay. Radio-labeled FLAG-HEN2 was incubated with cell lysates prepared from Neuro2a cells transfected with Myc-HES1 expression plasmid. The reaction mixture was immunoprecipitated with normal rabbit serum (NRS) or with polyclonal anti-Myc tag antibody and separated by SDS-PAGE followed by autoradiography. 1/5 inputs were also shown.
doi:10.1371/journal.pone.0019297.g005

It was reported that de-repression of *Mash1* might interfere with differentiation of sympatho-adrenal precursors of *Insm1* mutant mice although *Mash1* is expressed transiently in those cells during normal neural differentiation [15]. Furthermore, Watt et al. reported that N-myc positively regulates *Mash1* transcription [16]. Therefore, it is possible that in the transcriptional regulation of *Mash1*, LMO3 and HEN2 may associate with other nuclear factors like Insm1 and N-myc besides HES1.

From the developmental point of view, it is known that the LMO/HEN complex plays an important role in regulating neuronal differentiation [11,17]. As described [7,18], expression of *LMO3* was highly restricted in adult and fetal brains, and *HEN2* was expressed in developing nervous system. Genetic studies demonstrated that HEN2 participates in proper neural crest-derived neuroendocrine development and that Mash1 has a critical role in maintaining neuroendocrine cell phenotype [19,20]. Although *LMO3*-knockout mice did not exhibit any significant developmental defects, mice lacking both LMO1 and LMO3 died after birth, which might be due to neural defects [21]. Since neuroblastoma is one of the most common childhood solid tumors of peripheral nervous system arising from as yet unidentified population of neural crest cells [22] and Mash1 regulates proliferation of the sympathetic nervous system [23], it is likely that deregulated expression of Mash1 could contribute to genesis and development of neuroblastoma, which might be regulated by LMO3/HEN2 transcriptional complex both *in vitro* and *in vivo*. This LMO3/HEN2-HES1-Mash1 pathway could be the new future target for developing the anti-neuroblastoma treatment.

Materials and Methods

Ethics Statement

A hundred human neuroblastoma specimens used in the present study were kindly provided from various institutions and hospitals in Japan to the Chiba Cancer Center Neuroblastoma Tissue Bank. Written informed consent was obtained at each institution or hospital. This study was approved by the Chiba Cancer Center Institutional Review Board and were conducted according to the principles expressed in the Declaration of Helsinki.

Tumor Specimens

Tumors were classified according to the International Neuroblastoma Staging System (INSS); 25 Stage 1, 13 Stage 2, 33 Stage 3, 23 Stage 4, and 6 Stage4s. Clinical information including age at diagnosis, tumor origin, Shimada's histology, prognosis, and survival months of each patient were obtained. The median follow-up time for survivors was 35 months (range 3 to 91 months). Each tumor specimen was assayed for *TRKA* expression by Northern blot analysis and for *MYCN* amplification status by both fluorescence in situ hybridization (FISH) and real-time quantitative polymerase chain reaction (PCR).

Quantitative Real-time PCR

Total RNA prepared from primary neuroblastomas was reverse transcribed into cDNA (SuperScript II kit) and subjected to the real-time PCR. The expression level of *GAPDH* was measured in all samples to normalize *LMO3* and *Mash1* expression according to

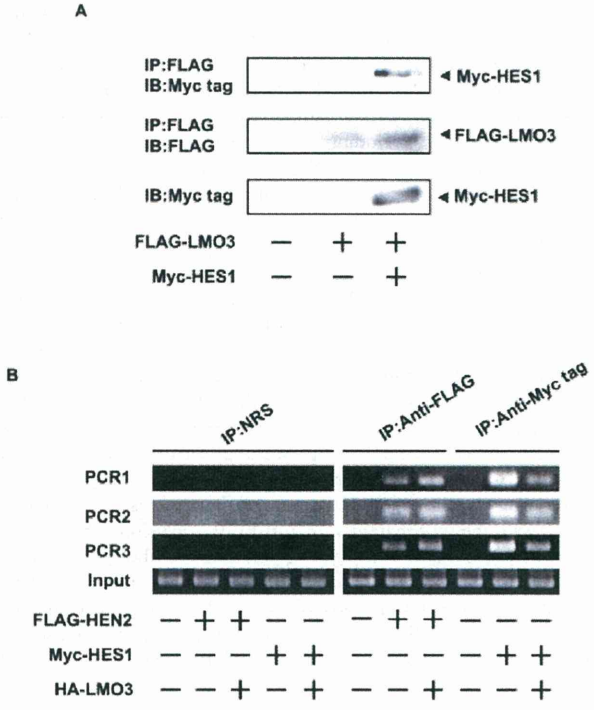

Figure 6. LMO3 attenuates binding of HES1 to Mash1 promoter and promotes that of HEN2. (A) Complex formation between LMO3 and HES1 in cells. Neuro2a cells were transiently transfected with the indicated combinations of the expression plasmids. Forty-eight hours after transfection, cell lysates were immunoprecipitated with anti-FLAG antibody followed by immunoblotting with anti-Myc tag antibody (top panel). Expressions of FLAG-LMO3 and Myc-HES1 are also shown (lower panels). (B) ChIP assay. Cross-linked chromatin prepared from Neuro2a cells transfected with the indicated combinations of expression plasmids was sonicated and immunoprecipitated with normal rabbit serum (NRS), polyclonal anti-Myc tag or with polyclonal anti-FLAG antibody. The genomic DNA was purified from the immunoprecipitates and amplified by PCR.
doi:10.1371/journal.pone.0019297.g006

the manufacturer's instructions (Applied Biosystems, Foster City, CA, USA). Oligonucleotide primers and TaqMan probes, which were labeled at the 5′ end with the reporter dye 6-carboxyfluorescein (FAM) and at the 3′ end with the quencher dye 6-carboxytetramethylrhodamine (TAMRA), were as follows: *LMO3*: forward 5′-TCTGAGGCTCTTTGGTGTAACG-3′, reverse 5′-CCAGGTGGTAAACATTGTCCTTG-3′ and probe 5′-FAM-AAACTGCGCTGCCTGTAGTAAGCTCATCC-TAMRA-3′. Taqman(R) Gene Expression Assay (Applied Biosystems) was purchased for *Mash1* with Assay ID Hs00269932-m1. Amplification and detection were done using the ABI Prism 7700 Sequence Detection System (Applied Biosystems).

Statistical Analysis

Student's *t* tests were used to explore possible associations between *LMO3* expression and other factors. The distinction between high and low levels of *LMO3* and *Mash1* expression was based on the mean value. Kaplan-Meier survival curves were calculated, and survival distributions were compared using the log-rank test. Cox regression models were used to explore associations among *LMO3* expression, *Mash1* expression, age, *MYCN* amplification, tumor origin, Shimada classification and survival. Statistical significance was declared if $P<0.05$.

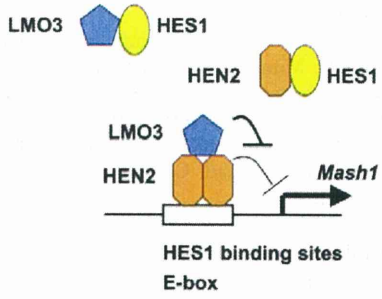

Figure 7. Model for LMO3 and HEN2 cooperation in transcriptional regulation of Mash1 in Neuroblastoma. HES1 binds to HES1 binding sites and E-box on *Mash1* promoter and represses *Mash1* transcription. LMO3 inhibits recruitment of HES1 onto HES1-binding sites and E-box on *Mash1* promoter by forming complex with HES1. HEN2 interferes with recruitment of HES1 onto HES1-binding sites and E-box on *Mash1* promoter by forming complex with HES1 and competing with HES1 in binding to these sites. LMO3 promotes recruitment of HEN2 onto HES1-binding sites and E-box on *Mash1* promoter by forming complex with HEN2 but inhibits negative effects of HEN2 on *Mash1* promoter. Thereby expression of *Mash1* is up-regulated.
doi:10.1371/journal.pone.0019297.g007

Cell Culture and Transfection

SH-SY5Y (human neuroblastoma, ATCC number CRL-2266), SK-N-BE (human neuroblastoma, ATCC number CRL-2271) and Neuro2a (mouse neuroblastoma, ATCC number CCL-131) cells were maintained in RPMI 1640 supplemented with 10% heat-inactivated fetal bovine serum at 37°C in an atmosphere of 5% CO_2 in the air. Cells were transfected with the indicated expression plasmids using Lipofectamine 2000 transfection reagent (Invitrogen, Carlsbad, CA, USA) as recommended by the manufacturer.

Generation of Recombinant Retroviral Vector and Retrovirus-mediated Gene Transfer

Human *Mash1* cDNA was subcloned into the *Hpa*I restriction site of the pLXSN vector. pLXSN or pLXSN- *Mash1* was transfected into the φ2 packaging cells, and SH-SY5Y cells (1×10^6 cells) infected with virus-containing culture medium were cultured in the medium containing 500 μg/ml G418 (Sigma Chemical Co., St. Louis, MO, USA). Two weeks after the selection in G418, drug-resistant clones were isolated and allowed to proliferate in medium containing G418.

Reverse Transcription-PCR Analysis

Total RNA was prepared from cultured cells by using the RNeasy Mini Kit (Qiagen, Valencia, CA, USA). Reverse transcription was carried out using random primers and SuperScript II (Invitrogen). Following the reverse transcription, the resultant cDNA was subjected to PCR-based amplification. PCR primers used were as follows: human *LMO3*, forward 5′-ATGCTCTCAGTCCAGCCAGA-3′ and reverse 5′-TCAGCGAACCTGGGGTGCAT-3′; human *HEN2*, forward 5′-AAGCAGCAGATTCGGACCAT-3′ and reverse 5′-CTTCTCCTCGCGGCTCAG-3′; human *Mash1*, forward 5′-GCGTTCAGCACTGACTTTTG-3′ and reverse 5′-CCCCGGGAGACTTCTTAGAG-3′; human *HES1*, forward 5′-TGAGCCAGCTGAAAACACTG-3′ and reverse 5′-GTCACCTCGTTCATGCACTC-3; human *glyceraldehydes-3-phosphate dehydrogenase* (*GAPDH*), forward 5′-ACCTGACCTGCCGTCTAGAA-3′ and reverse 5′-TCCACCACCCTGTTGCTGTA-3′.

RNA Interference Experiments

Human LMO3 RNAi vector was made using the original plasmid that is gift from A.K. Munirajan (Chiba Cancer Center Research Institute). The targeted sequence is 5′- GTAG-TAAGCTCATCCCTGC -3′. RNAi construct was transiently transfected into SH-SY5Y cells using Lipofectamine 2000 transfection reagent (Invitrogen, Carlsbad, CA, USA) according to the manufacturer's instruction.

Generation of Recombinant Adenoviral Vector

For construction of the adenovirus expression vector, an HA-tagged human LMO3 cDNA or a FLAG-tagged human HEN2 cDNA were inserted into the shuttle vector pHMCMV6 [24]. Efficient construction of a recombinant adenovirus vector by an improved *in vitro* ligation method [25]. The resultant shuttle vector was digested with I-CeuI and PI-SceI and subcloned into the identical restriction sites of the adenovirus expression vector pAdHM4. The recombinant adenovirus construct was digested with *Pac*I and transfected into 293 cells to generate recombinant adenovirus.

Luciferase Reporter Assay

The reporter plasmid contains a 1.2-kb fragment of the human *Mash1* promoter that was subcloned into the pGL3-Basic Vector (Promega Corp., Madison, WI, USA) upstream of the luciferase reporter gene. Cells were seeded in triplicates into 24-well plates (1×10^5 cells/well) 24 h prior to transfection. Cells were cotransfected with 100 ng of the reporter plasmid, 0.2 ng of pRL-CMV encoding *Renilla* luciferase cDNA, 5 ng of rat HES1expression vector, 150 ng of HA-LMO3, 100 to 300 ng of FLAG-HEN2 expression vectors. Total amount of plasmid DNA per transfection was kept constant with pcDNA3 (Invitrogen). At 48 h after transfection, luciferase activity was measured by a Dual-Luciferase Reporter Assay System (Promega), and the transfection efficiency was standardized against *Renilla* luciferase activity.

Chromatin Immunoprecipitation (ChIP) Assays

ChIP assay was performed according to the protocol recommended by Upstate (Lake Placid, NY, USA). Cross-linked chromatin prepared from Neuro2a cells transfected with expression plasmids was sonicated and immunoprecipitated with normal rabbit serum (NRS), polyclonal anti-Myc tag (Medical & Biological Laboratories, Nagoya, Japan) or with polyclonal anti-FLAG (Sigma, St. Louis, MO, USA) antibody. The genomic DNA was purified from the immunoprecipitates and amplified by PCR.

The primers used to amplify the mouse *Mash1* promoters were as follows: HES1 binding site (PCR-1), forward 5′-ATTTCTA-GAGCCACCCCCTG-3′ and reverse 5′-TTGTTGCAGTGCG-TGCGCC-3′; HES1 binding site (PCR-2), forward 5′-AGTGCGCTCGGCACTGACTT-3′ and reverse 5′-CGCG-GTTGGCTTCGGGAGCC-3′; E-box (PCR-3), forward 5′-ATGGAGAGTTTGCAAGGAGC-3′ and reverse 5′-CAGCCC-CACGCGCAGCCCTG-3′.

Western Blot Analysis and Immunoprecipitation

After transfection, Neuro2a cells were placed on ice, washed twice with phosphate-buffered saline, and lysed in lysis buffer containing 25 mM Tris-HCl (pH 8.0), 137 mM NaCl, 2.7 mM KCl, 1% TritonX-100, 1 mM phenylmethylsulfonyl fluoride and protease inhibitor mixture (Sigma). Lysates were placed on ice for 30 min, sonicated briefly, and clarified by centrifugation at 15,000× *g* for 5 min at 4°C. Protein concentrations of the supernatants were determined by using a Bio-Rad protein assay. For immunoblot analysis, proteins were resolved by sodium dodecyl sulfatepolyacrylamide gel electrophoresis (SDS-PAGE) and electrotransferred onto a nitrocellulose membrane. The membrane filter was blocked with 2% gelatin in Tris-buffered saline (TBS) for 3 h at room temperature and then incubated with a primary antibody including monoclonal anti-rat HES1 (Medical & Biological Laboratories, Nagoya, Japan), monoclonal anti-FLAG (M2; Sigma) or monoclonal anti-Myc (9B11; Cell Signaling Technology, Danvers, MA, USA) antibody over night at 4°C. The membrane filter was then incubated with a goat anti-mouse secondary antibody conjugated to horseradish peroxidase (Cell Signaling Technology, Danvers, MA, USA) or goat anti-rat secondary antibody conjugated to horseradish peroxidase (Beckman Coulter, Marseille, France) for 1 h at room temperature and bound secondary antibody was detected by enhanced chemiluminescence (Amersham Pharmacia Biotech) according to the manufacturer's protocol. For Immunoprecipitation, equal amounts of cell lysates (2 mg) were precleared with 25 µl of protein G-Sepharose (Amersham Bioscience, Uppsala, Sweden). After brief centrifugation, immunoprecipitation was carried out by incubating the supernatant with anti-FLAG polyclonal (Sigma, St. Louis, MO, USA) or anti-Myc tag polyclonal antibody (Medical & Biological Laboratories, Nagoya, Japan) over night at 4°C. Immunocomplexes were precipitated with protein G-Sepharose beads (Amersham Biosciences) for 3 hours at 4°C. The immunoprecipitated proteins were resolved by SDS-PAGE and analyzed by Western blotting.

In vitro Pull-down Assay

Radio-labeled FLAG-HEN2 was generated by using *in vitro* transcription/translation system (Promega) and incubated with cell lysates prepared from Neuro2a cells transfected with Myc-HES1 expression plasmid. The reaction mixture was immunoprecipitated with normal rabbit serum (NRS) or with polyclonal anti-Myc tag antibody (Medical & Biological Laboratories, Nagoya, Japan) and separated by SDS-PAGE followed by autoradiography.

Data Analysis and Statistics

All values for statistical significance represent mean ± SD. We carried out comparisons between means using the Student's *t*-test. Statistical significance implies $P<0.05$.

Supporting Information

Figure S1 Mash1-mediated growth promotion and LMO3/HEN2-mediated transcriptional induction of *Mash1* in SK-N-BE cells. (A) siRNA-mediated knockdown of LMO3. SK-N-BE cells were transfected with empty plasmid (4 µg) or with expression plasmid for siRNA targeting LMO3 (4 µg). Forty-eight hours after transfection, total RNA was prepared and analyzed for expression levels of *LMO3* and *Mash1* by RT-PCR. (B) Decreased growth rate in LMO3-knocked down cells. SK-N-BE cells (4.5×10^3 cells/well, 96 well culture plate) were transfected with empty plasmid (0.2 µg) or with expression plasmid for siRNA targeting LMO3 (0.2 µg). Forty-eight hours after transfection, cells were transferred into fresh medium. At the indicated time points, cell growth was measured by MTT assay (Cell Counting Kit-8, DOJINDO). (C) RT-PCR. SK-N-BE cells were transfected with pcDNA3 empty plasmid or with the indicated combinations of expression plasmid HA-LMO3 or FLAG-HEN2. At 72 hours after transfection, total RNA was analyzed for expression levels of *LMO3*, *HEN2* and *Mash1* by RT-PCR. *GAPDH* was used as an internal control. (D) siRNA-mediated knockdown of LMO3 reduces the promoter activity of *Mash1*. SK-N-BE cells were co-

transfected with constant amount of pluc-Mash1 (100 ng) and pRL-CMV (0.2 ng) in the presence or absence of increasing amounts of expression plasmid for siRNA against human LMO3 (100 or 400 ng). Forty-eight hours after transfection, cells were lysed and their luciferase activities were measured.
(TIF)

Figure S2 Expression of *LMO3*, *HEN2*, *Mash1* or *HES1* in neuroblastoma cell lines. Semiquantitative RT-PCR analysis for expression of *LMO3*, *HEN3*, *Mash1* or *HES1* in neuroblastoma cell lines is performed under linear amplification conditions. Expression of *GAPDH* is shown as a control.
(TIF)

Figure S3 Model for LMO3 and HEN2 cooperation in transcriptional regulation of *Mash1* in Neuroblastoma. (A) HES1 binds to HES1 binding sites and E- box on *Mash1* promoter and represses *Mash1* transcription. (B) LMO3 inhibits recruitment of HES1 onto HES1-binding sites and E-box on *Mash1* promoter by forming complex with HES1, and thereby inducing the expression of Mash1. (C) HEN2 interferes with recruitment of HES1 onto HES1-binding sites and E-box on *Mash1* promoter by forming complex with HES1 and competing with HES1 in binding to these sites. HEN2 also represses *Mash1* transcription but the inhibitory effects are weaker than that of HES1, and so up-regulating transcription of *Mash1*. (D) LMO3 promotes recruitment of HEN2 onto HES1-binding sites and E-box on *Mash1* promoter by forming complex with HEN2 but inhibits negative effects of HEN2 on *Mash1* promoter. Furthermore, LMO3 inhibits recruitment of HES1 onto HES1-binding sites and E-box on *Mash1* promoter, and so *Mash1* may be more highly expressed.
(TIF)

Table S1 Correlation between expression of LMO3 or Mash1 and other prognostic factors (Student's *t*-test).
(PDF)

Table S2 Univariate and multivariate analyses of Mash1 and LMO3 mRNA expression as well as other prognostic factors in primary neuroblastomas.
(PDF)

Acknowledgments

We are grateful to Dr. Ryuichiro Kageyama for providing the expression plasmid encoding HES1, to Drs. Nobutaka Hattori and Kaori Shiba for their valuable discussions. We also thank Yuki Nakamura for her technical assistance.

Author Contributions

Conceived and designed the experiments: EI AN. Performed the experiments: EI. Analyzed the data: EI MO SO. Contributed reagents/materials/analysis tools: YN AN. Wrote the paper: EI MO TO AN.

References

1. Nakagawara A (2004) Neural crest development and neuroblastoma: the genetic and biological link. In: Aloe L, Calzà L, eds. NGF and related molecules in health and disease, Progress in brain research. ELSEVIER. pp 14633–242.
2. Nakagawara A, Ohira M (2004) Comprehensive genomics linking between neural development and cancer: neuroblastoma as a model. Cancer Letters 204: 213–224.
3. Bach I (2000) The LIM domain: regulation by association. Mech Dev 91: 5–17.
4. Rabbitts TH (1998) LMO T-cell translocation oncogenes typify genes activated by chromosomal translocations that alter transcription and developmental processes. Genes Dev 12: 2651–2657.
5. Visvader JE, Venter D, Hahm K, Santamaria M, Sum EY, et al. (2001) The LIM domain gene LMO4 inhibits differentiation of mammary epithelial cells in vitro and is overexpressed in breast cancer. Proc Natl Acad Sci USA 98: 14452–14457.
6. Sum EY, Segara D, Duscio B, Bath ML, Field AS, et al. (2005) Overexpression of LMO4 induces mammary hyperplasia, promotes cell invasion, and is a predictor of poor outcome in breast cancer. Proc Natl Acad Sci USA 102: 7659–7664.
7. Aoyama M, Ozaki T, Inuzuka H, Tomotsune D, Hirato J, et al. (2005) LMO3 interacts with neuronal transcription factor, HEN2, and acts as an oncogene in neuroblastoma. Cancer Res 65: 4587–4597.
8. Gestblom C, Grynfeld A, Ora I, Ortoft E, Larsson C, et al. (1999) The basic helix-loop-helix transcription factor dHAND, a marker gene for the developing human sympathetic nervous system, is expressed in both high- and low-stage neuroblastomas. Lab Invest 79: 67–79.
9. Ichimiya S, Nimura Y, Seki N, Ozaki T, Nagase T, et al. (2001) Downregulation of hASH1 is associated with the retinoic acid-induced differentiation of human neuroblastoma cell lines. Med Pediatr Oncol 36: 132–134.
10. Kageyama R, Ohtsuka T, Kobayashi T (2007) The Hes family: repressors and oscillators that orchestrate embryogenesis. Development 134: 1243–1251.
11. Ramain P, Khechumian R, Khechumian K, Arbogast N, Ackermann C, et al. (2000) Interactions between chip and the achaete/scute-daughterless heterodimers are required for pannier-driven proneural patterning. Mol Cell 6: 781–790.
12. Asmar J, Biryukova I, Heitzler P (2008) *Drosophila* dLMO-PA isoform acts as an early activator of *achaete/scute* proneural expression. Developmental biology 316: 487–497.
13. Axelson H (2004) The Notch signaling cascade in neuroblastoma: role of the basic helix-loop-helix proteins HASH-1 and HES-1. Cancer Letters 204: 171–178.
14. Brown L, Baer R (1994) HEN1 encodes a 20-kilodalton phosphoprotein that binds an extended E-box motif as a homodimer. Mol Cell Biol 14: 1245–1255.
15. Wildner H, Gierl MS, Strehle M, Pla P, Birchmeier C (2008) Insm1 (IA-1) is a crucial component of the transcriptional network that controls differentiation of the sympatho-adrenal lineage. Development 135: 473–481.
16. Watt F, Watanabe R, Yang W, Agren N, Arvidsson Y, et al. (2007) A novel MASH1 enhancer with N-myc and CREB-binding sites is active in neuroblastoma. Cancer Gene Therapy 14: 287–296.
17. Bao J, Talmage DA, Role LW, Gautier J (2000) Regulation of neurogenesis by interactions between HEN1 and neuronal LMO proteins. Development 127: 425–435.
18. Bagley CG, Lipkowitz S, Gobel V, Mahon KA, Bertness V, et al. (1992) Molecular characterization of NSCL, a gene encoding a helix-loop-helix protein expressed in the developing nervous system. Proc Natl Acad Sci USA 89: 38–42.
19. Good DJ, Porter FD, Mahon KA, Parlow AF, Westphal H, et al. (1997) Hypogonadism and obesity in mice with a targeted deletion of the Nhlh2 gene. Nat Genet 15: 397–401.
20. Lanigan TM, DeRaad SK, Russo AF (1998) Requirement of the MASH-1 transcription factor for neuroendocrine differentiation of thyroid C cells. J Neurobiol 34: 126–134.
21. Tse E, Smith AJ, Hunt S, Lavenir I, Forster A, et al. (2004) Null mutation of the Lmo4 gene or a combined null mutation of the Lmo1/Lmo3 genes causes perinatal lethality, and Lmo4 controls neural tube development in mice. Mol Cell Biol 24: 2063–2073.
22. Brodeur GM (2003) Neuroblastoma: biological insights into a clinical enigma. Nat Rev Cancer 3: 203–216.
23. Morikawa Y, Zehir A, Maska E, Deng C, Schneider MD, et al. (2009) BMP signaling regulates sympathetic nervous system development through Smad 4-dependent and -independent pathways. Development 136: 3575–3584.
24. Mizuguchi H, Kay MA (1998) Efficient construction of a recombinant adenovirus vector by an improved *in vitro* ligation method. Hum Gene Ther 9: 2577–2583.
25. Mizuguchi H, Kay MA (1999) A simple method for constructing E1- and E1/E4-deleted recombinant adenoviral vectors. Hum Gene Ther 10: 2013–2017.